Expansion of Working Memory Capacity Supports Early Skill Learning

Fumiaki Iwane[1], William Hayward[1], I. M. Dushyanthi Karunathilake[1],

Ethan R. Buch[1], and Leonardo G. Cohen[1,*]

[1]Human Cortical Physiology and Neurorehabilitation Section, NINDS, NIH, USA

*To whom correspondence should be addressed

cohenl@ninds.nih.gov

This research was supported by the Intramural Research Program of the National Institutes of Health (NIH). The contributions of the NIH author(s) are considered Works of the United States Government. The findings and conclusions presented in this paper are those of the author(s) and do not necessarily reflect the views of the NIH or the U.S. Department of Health and Human Services.

Abstract

Real-world motor skills depend on the precise spatiotemporal coordination of action sequences refined through practice. Working memory, which transiently maintains and manipulates task-relevant information, supports skill acquisition expanding with extensive training, as shown in expert domains such as in master chess players. Yet, the temporal dynamics of working memory emergence and expansion during the rapid performance gains that define early skill learning remain unclear.

We addressed this question across three experiments in which participants learned various naturalistic sequential keypress skills. Within each practice trial, we observed segments of high-initial-skill (HIS)—transient periods of elevated performance followed by skill drops—that persisted throughout training. The keypress content of HIS segments scaled with execution speed and systematically increased with practice, reflecting an expansion of keypress chunk content consistent with the progressive enlargement of working memory capacity. Importantly, HIS segment keypress content continued to rise even after overall performance plateaued. Theta–gamma phase–amplitude coupling (θ/γ PAC) and beta (β)-band bursts, mechanisms implicated in maintaining and binding individual actions into sequences in working memory, were elevated during HIS segments with hippocampal θ/γ PAC predicting HIS segment content.

Our results suggest that working memory capacity expands during early learning of a naturalistic skill and continues strengthening with practice after skill plateau is reached, possibly supported by hippocampal theta/gamma phase-amplitude coupling.

Introduction

Working memory (WM) holds and processes information for short periods of time[1,2]. Functional Magnetic Resonance Imaging (fMRI) and Electroencephalography (EEG) have revealed the activation of regions strongly associated with WM function, notably the hippocampus[3] and the prefrontal cortex, during motor learning tasks[4,5] while temporal disruption of the prefrontal cortex with transcranial magnetic stimulation (TMS) causally impairs learning[6]. Further indication of the link between skill acquisition and WM has been the finding that WM capacity correlates with the speed of task execution[2] and the rate or progress of motor sequence[7] and reinforcement learning[8-10]. This relationship has been further substantiated by the finding that performance of standardized WM tasks alongside training to learn a new skill interferes with skill learning [7,11].

WM capacity can expand in the context of extended practice[1,7,12]. Grouping individual units of information together into chunks[8,13] (e.g., a phone or a pin number) is one way in which WM capacity can expand[8]. Thus, chunking simplifies task retrieval and execution when the number of individual action items exceeds the constraints of WM capacity (3-7 elements)[14-17]. With prolonged training, WM capacity can expand by increasing the number of individual action items contained in any given chunk (i.e., chunk content) as observed for example in Master chess players[18]. In contrast to the documented WM expansion after extended practice, it is not known if WM capacity can expand nor its time course during the rapid initial performance improvements of skill learning[19]. In the context of early procedural learning, WM could theoretically support storage of information[20], sensorimotor integration[21], recall of task details and instructions[22] and retrieval of procedural steps before automaticity is reached[11].

The WM contribution to early learning could be expressed as within-practice segments of high initial skill (HIS) interrupted by skill drops reflective of depletion of the WM buffer. Specifically, the number of keypresses within these HIS segments may serve as a behavioral expression of the WM capacity for the practiced skill in any given practice trial. One would then expect more numerous individual action items within HIS segments learning fast than acquiring slow, more difficult, skills[2]. Further, an increase in individual action items contained within HIS segments or chunks[1,12,23] with advancing training would point to expansion of WM capacity. On the other hand, reactive inhibitory factors like motor fatigue[24-26] could negatively impact measures of memory function.[27] In this scenario, reduction in HIS segment duration or in individual content within HIS segments or chunks with advancing practice would point to a motor[24-26] fatigue rather than a WM origin[28].

At a neural level, theta (θ, 4-8Hz)/gamma (γ, >25Hz) phase amplitude coupling (θ/γ PAC) is a mechanism supportive of WM function[29]. θ/γ PAC refers to the recurrence of identical sequences of γ bursts representing sequential memory items during specific phases of the θ rhythm [30-32]. θ/γ PAC aids in binding individual action representations into coherent sequences in WM. Consistently, θ/γ ratios predict behavioral measurements of memory span[33] and correlate with WM capacity[34]. β burst oscillatory rhythms have been also linked

to WM function[35-37]. Thus, higher θ/γ PAC and β burst oscillatory activity[38-40] during HIS segments could reflect a WM origin.

Here, we investigated the WM contribution to early skill learning over a series of experiments in which subjects learned naturalistic sequential keypress skills. We report that (a) periods of high initial skill (HIS) emerged indeed during individual practice trials of early learning across three skills of different speeds, (b) the content of HIS segments (number of individual keypress actions/HIS) was larger learning fast skills than slow, more difficult ones, (c) both the HIS keypress contents (number of keypresses/HIS segment) and chunk (number of keypresses/chunk) contents increased with practice in all three tasks, and (d) theta–gamma phase–amplitude coupling (θ/γ PAC) and beta (β)-band bursts—oscillatory mechanisms implicated in binding actions into WM sequences—were elevated during HIS segments, with hippocampal θ/γ PAC predicting HIS segment content.

Results

In the first experiment (N=2,152), we characterized the relative duration of all possible 6-item keypress sequences by adding their keypress transition times (KTT) components along a naturalistic skill speed index (SSI). Healthy volunteers typed 16 different keypress pairs using four fingers of their left, non-dominant hand (little, ring, middle, and index fingers) in a pseudorandom order (**Fig 1A**). Within-subject z-normalized keypress transition times (KTTs) were measured for all pairs and a matrix showing median z-score shifts for each KTT pair was built (**Fig 1B**). This information was used to estimate the duration of all possible 6-item keypress sequences by adding their KTT components (**Fig 1C**).

In Experiment 2 (n=404), we evaluated learning dynamics of three skills (i.e. keypress sequences) with different speed profiles: slow [SSI=0.07, N=122], medium [SSI=0.41, N=127] and fast [SSI=0.50, N=158], **Fig 1C, D**). Subjects were randomly assigned to practice one of the skills over 26 trials. Each trial consisted of 10 seconds of practice followed by 10 seconds of rest[19]. Participants were instructed to perform the skill as fast and accurately as possible.

Segments of high initial skill (HIS) were identified in all groups

Practice led to rapid behavioral gains across all skill groups, with greater improvements observed in participants practicing faster skills compared to slower ones (**Fig 2A**). Consistent within-trial performance profiles, characterized by a high initial skill (HIS) segment followed by a rapid skill drop, emerged between trials 3 and 5 and remained present until the end of training (**Fig 2A,** arrows; **Fig S1A**). We fit a double-sigmoid function to individual trial performances to characterize within-trial skill plateaus, gains, and drops (**Fig 2B** and **Fig S2**). The end of HIS segments for each individual trial was defined as the point of maximum deceleration of the skill drops (**Fig 2B, C** circles). Within-subject and -trial modelled curves were then aligned to the end of HIS segments revealing the consistency of this pattern (**Fig 2C** and **Fig S3**). We observed that the duration of HIS segments was longer when learning faster skills (fast: 4.72±0.05s) compared to slower ones

(medium: 4.18±0.07 and slow: 4.14±0.07s, one-way ANOVA, $F_{2,404}$=30.5, p=4.54×10^{-13}, **Fig S4A**).

HIS segment keypress content scaled with speed of skill practice

A possible cause of within-trial skill drops at the end of HIS segments is motor fatigue [24-26,41]. In this framework, each keypress incrementally contributes to fatigue, while recovery occurs in proportion to the separation between individual keypresses, keypress transition times (KTT)[42]. Thus, when skills are executed rapidly, the resultant shorter KTTs allow less recovery between keypresses, leading to greater cumulative fatigue. As a result, faster skills would be expected to elicit shorter HIS segments with fewer keypresses compared to slower skills, where longer KTTs permit more recovery. We found the opposite. HIS segment keypress content increased progressively with skill speed: 10.83±0.32, 12.63±0.46 and 18.86±0.51 keypresses/HIS segment learning the slow, medium and fast skills, respectively (one-way ANOVA, $F_{2,404}$=89.8, p=5.37×10^{-33}, **Fig 3A**), all values beyond the number of keypresses that can be preplanned[43]. Keypress rates also increased progressively with skill speed (2.59±0.07, 2.98±0.10 and 3.92±0.10 keypresses/s for slow, medium and fast skills, respectively; one-way ANOVA, $F_{2,404}$=55.8, p=3.89×10^{-22}, **Fig S4B**). Crucially, HIS segments were absent during the practice of four pseudo-randomized sequences, all of which were performed at speeds similar to the medium sequence in the main study (**Fig S5**). Thus, HIS segment keypress content scaled with speed of practice, yet remained absent practicing non-repeating sequences, both findings inconsistent with a motor fatigue origin.

Training increased the HIS segment keypress content across skill groups

Next, we measured training effects on the HIS segments' content. We reasoned that accumulating fatigue in the course of practice[41] would express as a reduction in HIS segment content as training progressed. Again, we found the opposite. HIS segments keypress content increased, rather than decreased, as training progressed in all skill groups (linear-mixed effects models [LMM], BHFDR corrected, Slow: $F_{1,2633}$=32.0, t_{2633}=5.65, p=5.14×10^{-8}, Medium: $F_{1,2663}$=21.9, t_{2663}=4.68, p=4.53×10^{-6}, Fast: $F_{1,3201}$=5.90, t_{3201}=2.43, p=0.015, **Fig S4C**) in the absence of changes in HIS segment duration (Slow: $F_{1,2750}$=0.28, t_{2750}=0.53, p=0.99, Medium: $F_{1,2787}$=2.57×10^{-4}, t_{2787}=0.02, p=0.99, Fast: $F_{1,3357}$=1.75×10^{-3}, t_{3357}=0.04, p=0.99, **Fig 3B**). Keypress rates within HIS segments also increased progressively with training in all skill groups (Slow: $F_{1,2629}$=143.0, t_{2629}=12.0, p=3.90×10^{-32}, Medium: $F_{1,2660}$=121.2, t_{2660}=11.0, p=1.34×10^{-27}, Fast: $F_{1,3199}$=43.8, t_{3199}=6.62, p=4.15×10^{-11}, **Fig 3C**). These results held when the analysis was restricted to the plateau phase of the learning curves, where virtually no further performance improvements were observed (trial 6-26, **Fig S6A**). Thus, HIS segment content continues to expand with advancing training even after speed plateaus, consistent with a progressive expansion of effective WM capacity supporting the practiced skills rather than a reflection of accumulating fatigue.

Training-dependent enrichment of HIS segments is contingent upon the expansion of motor chunk content

Memory capacity can expand by grouping units of information together into single entities or chunks (e.g., a phone or pin numbers)[8,13]. Next, we investigated the possibility that changes in chunking organization could inform HIS segment dynamics. Hierarchical clustering was used to identify boundaries between chunks of keypresses during HIS segments (**Fig 3D** and **Fig S7**). Chunk boundaries were identified when the duration of keypress pairs within a skill sequence (KTT_{seq}) exceeded the corresponding durations of the same pairs performed outside the sequence context (KTT_{pairs}) within the same individual. A chunking structure was identified in HIS segments of all skill groups. We found a comparable number of chunks/HIS segment across skills (Slow: 7.13±0.30, Medium: 7.78±0.37, and Fast: 7.87±0.34 chunks/HIS segment, one-way ANOVA, $F_{2,404}$=1.33, p=0.27, **Fig 3E** and **Fig S8A**), reminiscent of known boundaries in WM function ("rule of 7")[14-17]. On the other hand, the overall chunk content (keypresses/chunk) was larger learning fast than medium or slow skills (Slow: 1.93±0.10, Medium: 1.95±0.08, and Fast: 3.84±0.26 keypresses/chunk, one-way ANOVA, $F_{2,404}$=36.5, p=2.61×10^{-15}, **Fig S9A**). Importantly, the chunk content increased progressively with training in all skill groups (Slow: $F_{1,2630}$=72.1, t_{2630}=8.49, p=5.15×10^{-17}, Medium: $F_{1,2662}$=81.5, t_{2662}=9.03, p=9.73×10^{-19}, Fast: $F_{1,3200}$=9.03, t_{3200}=3.00, p=0.003, **Fig 3F**) and these results persisted when the analysis was restricted to the plateau phase of the learning curve (trials 6-26, **Fig S6B**). Thus, training expanded chunk content during HIS segments across skills. Altogether, behavioral results up to this point are consistent with the view that HIS segment dynamics during initial learning reflect the expansion of a working memory buffer, rather than content reductions caused by motor fatigue.

In the next experiment (Experiment 3, N=32), we evaluated subjects learning a medium speed sequential skill task in a magnetoencephalography (MEG) lab[19]. The purpose was two-fold. To determine the reproducibility of the findings reported in Experiment 2 and to evaluate physiological markers of WM during HIS segments. Behavioral findings were indeed very similar to those reported learning the medium speed skill in Experiment 2. Performance curves revealed the emergence of HIS segments starting at trial 5 and persisting till the end of training (**Fig S10**). The number of keypresses in HIS segments (14.07±0.91) increased as training progressed (LMM, $F_{1,985}$=9.00, t_{985}=3.0, p=$3.0\text{x}10^{-3}$, **Fig S11A**) as did keypress rates ($F_{1,985}$=104.2, t_{985}=10.21, p=2.5×10^{-23}, **Fig S11C**) in the absence of changes in HIS segment duration ($F_{1,1020}$=1.21, t_{1020}=-1.10, p=0.27, 4.10±0.11, ≈4.0 sec, **Fig S11B**). Thus, training-dependent expansion of content within HIS segments was reproducible across experiments 2 and 3.

Increased θ/γ PAC and β band bursting rates during HIS segments of early learning

Next, we evaluated θ/γ PAC[29,44,45]. Whole-brain source-space θ/γ PAC (**Fig S12A**) was significantly higher during HIS segments (trials 5-36) than during the same time window in trials preceding the emergence of HIS segments (trials 1-4, paired t-test, t_{31}=-2.95, p=0.006, **Fig 4A**). Source-space parcellated θ/γ PAC during HIS segments was higher relative to its time-shifted surrogates in contralateral hippocampus, insula and orbitofrontal cortex, bilateral ventromedial prefrontal cortex, and ipsilateral parieto-occipital regions (cluster-forming threshold t>2.74 and distance<20mm, number of permutations=2,000, p<0.01, **Fig 4B**). θ/γ PAC in these regions was significantly higher during HIS segments of practice trials

than during post-HIS intervals of the same trials (paired *t*-test, BHFDR corrected, **Fig 4C** and **Fig S12B**). Importantly, hippocampal θ/γ PAC strongly predicted HIS segment content (keypresses/HIS segment; LMM, $F_{1,986}$ =13.5, t_{986}=3.68, p=9.89×10^{-4}, **Fig 4D**) and skills (**Fig S15B**).

We then evaluated transient high-power bursts. We found higher β band burst rates during HIS segments than during post-HIS intervals of the same trials (whole-brain MEG sensor-space, HIS segments defined in each trial and each participant, cluster-forming threshold t>3.37, number of permutations=2,000, p<0.01, **Fig 5A**). We did not find differences in bursting rates in other frequency bands. β burst rates were higher in trials with HIS segments (trials 5-36, group-averaged HIS segments) than in the same time window of trials preceding the emergence of HIS segments (trials 1-4, **Fig 5B**). Finally, source-space parcellated β burst rates were significantly higher during HIS segments of practice trials than during post-HIS intervals of the same trials in bilateral insula and frontal, temporal and anterior cingulate cortices (cluster-forming threshold t>3.37 and distance<20mm, number of permutations=2,000, p<0.01, **Fig 5C**).

DISCUSSION

We report that during procedural skill memory formation, a reproducible performance pattern of high initial skill (HIS) segments immediately followed by rapid slowing emerges within individual practice trials. The number of sequential keypress actions occurring within these HIS segments (i.e. - their content) was greater for fast rather than slow learning skills. Notably, HIS segment keypress content increased progressively with training, with more actions becoming integrated into single performance chunks, both findings inconsistent with a motor fatigue-based[24-26] explanation. Importantly, neural activity during HIS segments showed elevated θ/γ phase–amplitude coupling (PAC) and β-band bursts across memory-related neocortical and medial temporal regions, with hippocampal θ/γ PAC strongly predicting HIS segment content.

HIS segment content is not explained by motor fatigue

The skill speed increases with practice and with task familiarity in humans[46-48] and non-human-primates[47,49]. Speed of execution is influenced by task difficulty[50-52] and the biomechanical characteristics of the human hand[53], as well as by surround inhibition between individual finger representations in the motor cortex[54], all factors which constrain movement individuation and dexterity. Since skill speed could interact with WM capacity[46-48] as well as with inhibitory influences like motor fatigue [24-26,28], we evaluated its impact on early procedural learning. We developed a skill index (Exp 1) to estimate the speed of execution of all possible 6-item keypress sequences (**Fig 1**). Next, we evaluated learning dynamics of three different naturalistic skills ranging from slow to fast (Exp 2) following an experimental paradigm previously described.[55] A double-sigmoid function was fit to individual trial performance curves to capture within-trial skill plateaus, gains, and declines. For each trial, the end of a high-initial-skill (HIS) segment was defined as the point of

maximum deceleration during the ensuing rapid performance drop (**Fig 2B,C**, circles; **Fig S2**).

Practice led to prominent initial performance improvements followed by a phase in which average skill stabilized, limiting further gains once near-ceiling proficiency was achieved. We found that segments of HIS interrupted by skill drops emerged after the initial training trials (practice trials 3 to 5 depending on skill speed) and persisted along the plateau period in all subjects and skill groups. We and others have attributed these performance drops to fatigue accumulating with continued practice[19,56], particularly during the execution of fast motor tasks[41,56]. Under this scenario, each keypress results in some amount of fatigue that is recovered from during the "resting" time between keypresses (KTT)[41,57]. We reasoned that if this were the case, HIS segment content should be smaller when learning fast skills (containing more fatigue-inducing keypresses combined with shorter recovery time intervals) than for slower skills (fewer keypresses combined with longer recovery time intervals). Contrary to this prediction, we found that the keypress content of HIS segments was larger for faster skills compared to slower ones, ranging between 18 and 10 keypresses (**Fig 3A**), and predicted skill performance (**Fig S15A**).

One would also expect that the accumulation of motor fatigue[24-26,41] in the course of training would result in slower typing speed and/or earlier skill drops, leading to shorter HIS segment durations with diminished keypress content. Contrary to these predictions, we observed a training-dependent expansion of HIS segment keypress content, with no accompanying change in HIS segment duration across all skills tested (**Fig 3**, **Fig S4C** and **Fig S11A**). These findings are inconsistent with a fatigue-based explanation of HIS content, aligning instead with reports that motor fatigue requires practice periods longer (10–60 min) than those used in this study (<9 min)[58-60]. Thus, motor fatigue does not play a pivotal role in shaping HIS segment dynamics during the early stages of mastering a naturalistic sequential skill.

HIS segment content informs on working memory capacity during early skill learning

Alternatively, HIS segment dynamics could inform on WM capacity during early procedural learning. We found that, depending on skill speed, HIS segments comprised between 10 and 18 keypress actions (**Fig 3A**), vastly exceeding the 2-3 keypresses that can be preplanned in the context of skill learning[43]. Interestingly, 10-18 keypress actions also exceed the typical capacity limits of WM (3–7 items)[14-16], suggesting that individual keypresses are unlikely to constitute the fundamental units of sequential skill memory as training progresses.

To address this possibility, we investigated the chunking organization of HIS segments content. As a new motor skill is learned, individual actions are grouped into "chunks", which simplify sequential execution and memory storage in situations where the number of sequence actions exceeds the constraints of WM capacity[23]. Examples of memory chunks in daily life are phone numbers or passwords, which are commonly recalled as single memory units rather than as the sum of the individual numbers or letters. We used hierarchical clustering to determine the boundaries of skill sequence chunks, each one preceded and followed by long keypress transition times (KTT)[61-63]. Within any given chunk,

KTTs recorded in the context of the skill sequence (KTT_{seq}) were equal or faster than KTTs recorded in a non-sequential skill context (KTT_{pairs}, **Methods**)[61,64,65].

The key finding from this analysis was that the number of chunks per HIS segment was strikingly consistent across skill groups—ranging between 7 and 8 (**Fig 3E**)—aligning closely with the canonical WM capacity described by Miller's rule (rule of 7)[14-17]. Thus, keypress chunks rather than individual keypresses may represent the skill memory "units" as a new skill is acquired. Next, we examined how practice influenced the keypress content of chunks. Across all skill levels, chunk content (keypresses/chunk) expanded with training rather than contracting (**Fig 3F**), a pattern inconsistent with a fatigue-based account. Notably, HIS segment content continued to expand even during the plateau phase of the learning curves, despite overall performance reaching near-ceiling levels and despite presumably accumulating motor fatigue (**Fig S6**). Altogether, these results are consistent with the expansion of WM capacity during early procedural learning[66].

θ/γ PAC and β-band bursts in memory-related and sensorimotor integration regions during HIS segments

Which neural mechanisms might support the expansion of WM capacity during early learning? One candidate is theta–gamma phase–amplitude coupling (θ/γ PAC), which has been implicated in binding individual actions into coherent sequences[34,67-75] and in the active maintenance of information within WM[29,44,45]. Our observation of elevated θ/γ PAC during HIS segments suggests that this coupling may facilitate the integration of individual finger representations—reflected in low frequency γ bursts[76]—into precise temporal and spatial positions within slower θ oscillations (i.e. precession), thereby encoding the identity of emerging sequences and chunks[34,67-75]. This binding mechanism, operating during motor execution, is likely reinforced during rapid consolidation periods that develop across rest intervals interspersed with practice[19]. Contributors to rapid consolidation during these rest periods of early skill learning include wakeful neural replay[77,78] and contextualization of individual sequence action representations[55].

Elevated θ/γ PAC during HIS segments was observed across a distributed network encompassing memory-related and sensorimotor integration regions (including the hippocampus, insula, orbitofrontal, prefrontal cortex, and regions within parieto-occipital and intraparietal sulci). The hippocampus emerged as a key node, as θ/γ PAC in this region strongly predicted HIS segment content (**Fig 4D**) and actual skill (**Fig S15B**). This observation aligns with evidence implicating hippocampo–neocortical neural replay[19,77,79-82] and hippocampal ripples—established biomarkers of replay events[83]—in supporting micro-offline performance gains during early phases of skill acquisition[78,84,85]. Altogether, these findings converge with the well-documented role of the hippocampus in supporting both working[3], and procedural[77,79,86] memory formation.

Finally, we evaluated broadband neural oscillatory features associated with HIS segment content. The only frequency band differentiating transient high-power bursts during HIS versus post-HIS segments was β band, which revealed elevated burst rates during HIS segments particularly in the insula and frontal, temporal and anterior cingulate cortices.

Furthermore, whole-brain β burst rates were higher in trials after HIS segments had become clearly defined (trials 5-36) than in trials preceding the emergence of HIS segments (trials 1-4). These results are in line with previous work showing that high β oscillatory activity[38], organized predominantly in bursts[39,40,87], supports WM function. Thus, higher θ/γ PAC and β burst oscillatory activity during HIS segments constitute possible mechanisms supportive of the build-up and expansion of WM content during early learning of naturalistic sequential skills.

Limitations and future directions

While behavioral results were generalizable to three different naturalistic self-paced skills and reproducible across two experimental platforms (online and in-lab), it would be important in the future to evaluate generalizability to other tasks (e.g., inhibitory factors, such as fatigue, have a substantially greater impact on reaction-time tasks relative to the self-paced naturalistic skills utilized in our study (see Eysenck, 1965[88])[89]. Another compelling avenue for future research is the relationship between WM and preplanning. In our study of naturalistic skill learning, WM capacity across the three skills tested spanned approximately 10–18 keypresses organized into roughly seven chunks—well beyond the more limited 2–4 keypresses that can typically be preplanned during sequence learning[43]. It is therefore possible that effective preplanning emerges as WM capacity expands with practice, an issue for future investigation. We assessed neural substrates of HIS segment content learning a medium-speed task. Future work could expand this mechanistic investigation to skill tasks of different speeds. Finally, we cannot exclude the possibility that reactive inhibitory mechanisms like motor fatigue may exert a greater influence on HIS segment dynamics during longer or more effortful training protocols than those examined here.

In summary, our findings suggest that early procedural formation of a naturalistic memory may be contingent upon a gradual augmentation of working memory capacity, as evidenced by the content of HIS segments. Notably, this increase persists even after the overall skill performance reached a plateau. Elevated θ/γ PAC and β-band burst rates across memory-related neocortical and medial temporal regions, particularly hippocampal θ/γ PAC, emerged as candidate neural mechanisms supporting this expansion and skill gains.

Acknowledgments

We thank Ms. Tasneem Malik, Ms. Michele Richman, Ms. Catherine Blumhorst and NIMH MEG Core Facility staff for their support. This work utilized the computational resources of the NIH HPC Biowulf cluster (http://hpc.nih.gov). FI was partly supported by KAITOKU fellowship funded by the Japan Society for the Promotion of Science (JSPS). This research was supported by the Intramural Research Program of the National Institutes of Health (NIH). The contributions of the NIH author(s) are considered Works of the United States Government. The findings and conclusions presented in this paper are those of the author(s) and do not necessarily reflect the views of the NIH or the U.S. Department of Health and Human Services.

Author Contributions

Conceptualization: F.I., E.R.B. and L.G.C.; Methodology: F.I., E.R.B. and L.G.C.; Formal Analysis: F.I., E.R.B. and L.G.C.; Investigation: F.I., E.R.B. and L.G.C.; Writing—original draft: F.I., E.R.B. and L.G.C.; Writing—review & editing: F.I., W.H., D.K., E.R.B. and L.G.C.; Visualization: F.I., E.R.B. and L.G.C.; Supervision: E.R.B. and L.G.C.

Data and Code availability

Behavioral data collected in Experiment 1 and 2 will be available upon publication. De-identified data used in Experiment 3, permanently unlinked from all personal identifiable information (PII), are available (https://openneuro.org/datasets/ds006502/versions/1.0.0). The preprocessed data and analysis scripts used to generate the results in this study will be available upon publication.

Declarations of Interest

The authors declare no competing interests.

METHODS

Participants

Right-handed participants performed a well-established sequential motor learning task[90,91] consisting of repetitive typing of keypress sequences with their non-dominant, left hand. The study consisted of three experiments: Experiments 1 (n=2152, 1043 women, mean age 28.1±0.12) and 2 (n=404, 199 women, mean age 28.1±0.26) were performed online, while all Experiment 3 (n=32, 16 women, mean age 26.6±0.87) procedures were carried out at the National Institutes of Health (NIH) Clinical Center. The study was approved by the NIH Institutional Review Board (IRB). All online subjects (Experiments 1 and 2) were recruited from the Connect crowd-sourcing platform (Prime Research Solutions LLC, NY, USA) and completed a digital acknowledgement of participation before engaging in study procedures. In Experiment 2, participants were excluded if they performed the task with their right hand, typed the sequence only once per practice trial, or exhibited a task inactivity period of five seconds or more in more than four practice trials (n=194). Participants for the in-person study (Experiment 3) signed informed consent preceding testing.

Task

In Experiment 1, we collected a very large sample (n=2152) of independent keypress transition time (KTT) data, which was used to synthesize predictive estimates of the relative speed of all possible 6-item keypress skill sequences. We refer to these estimates as the naturalistic Skill Speed Index (SSI). Participants performed a task in which they executed all 16 possible two-finger keypress transitions using four fingers (little, ring, middle, and index) of their non-dominant, left hand. Keypresses were made on a standard computer keyboard. On each trial, a pair of numeric cues (e.g. 24) corresponding to a specific pair of finger keypresses (1=little, 2=ring, 3=middle finger, 4=index finger) were presented, and participants were instructed to respond as quickly and as accurately as possible (**Fig 1A**). Individual numbers were replaced with "X" as correct keypresses were executed. In the event of an incorrect response, the trial was repeated until executed correctly. The inter-trial interval was uniformly varied between 200–500ms. Each transition was sampled a total of five times, and their presentation order was pseudorandomized.

In Experiment 2, we evaluated learning dynamics of three keypress skill sequences with different predicted speed profiles: slow, medium and fast, **Fig 1C**). Participants completed the pseudorandomized paired keypress task described for Experiment 1 before and after the sequential motor skill learning task (**Fig 1D**). Training comprised trials alternating between 10 s of practice and 10 s of rest—adhering closely to the methodological recommendations of Pan and Rickard (2015) to minimize reactive inhibition[56]. Keypress timing and finger identity were recorded on each trial, and skill was quantified as the speed of correctly executed sequences (keypresses per second)[19]. Participants, instructed to perform the sequential skill as fast and accurately as possible, were randomly assigned to practice one

of the three skill sequences tested (**Fig 1C**). Skill sequences were displayed along the practice intervals. A small dot appeared after each keypress, signaling the participants' present position within the sequence. Following the completion of a full sequence iteration, the dot returned to the first sequence item. No feedback was provided. During rest intervals, each sequence item was replaced with an "X", and the dot disappeared.

Experiment 3 was carried out in-person in the NIH magnetoencephalography (MEG) lab. Subjects practiced the medium-speed sequential skill 4-1-3-2-4 over alternating 10 seconds of practice interleaved with 10 seconds of rest for 36 trials. Subjects used an MEG-compatible response pad (Cedrus LS-LINE, Cedrus Corp.) to record keypresses.

Behavioral Data Analysis

Skill Speed Index

The naturalistic SSI was derived from z-normalized transition times within each individual (**Fig 1B**). Positive values corresponded to relatively fast transitions (e.g., 4–4, 3–3, 2–3), whereas negative values reflected slower transitions (e.g., 1–3, 4–2, 2–4). For each sequence, the SSI was obtained by summing the corresponding transition scores and subsequently applying min–max normalization across all possible sequences. Sequences lacking all four keypress identities were excluded from further analyses (**Fig 1C**).

Skill Measurement

We quantified performance by measuring the time required to complete each sequence cycle accurately and calculating the rate of correct keypresses per second (keypresses/sec). To isolate learned sequence execution, we excluded the initial reaction time (from practice trial onset to the first keypress) and any transitions containing errors, encompasses prolonged transition times[92]. A keypress was considered correct if it matched any circular shift of the target sequence, ensuring that valid transitional elements were retained for skill estimation. Skill values derived from individual correct keypresses were then interpolated and extrapolated to yield a continuous, millisecond-resolution measure of skill across the entire practice interval.

Within-practice Skill Dynamics

First, we identified practice trials depicting time windows of high initial skill (HIS segments). Within-trial skill changes were calculated as the difference in correct sequence speed between the beginning and end of each practice trial (**Fig S1A** and **Fig S10B**), which were characterized by a regression model that includes an offset, and an exponential term:

$$L(t) = C_1 + C_2 \cdot \left(1 - e^{-\lambda t}\right) \quad (1)$$

where $L(t)$ represented the group averaged within-trial skill change on practice trial, t, C_1 and C_2 controlled the initial performance and asymptote of the exponential term, and λ

controlled the rate of change. Parameters $C_1 \in [0,5]$, $C_2 \in [-5,5]$, and $\lambda \in [0,2]$ were estimated using a constrained nonlinear least-squares method (*lsqcurvefit.m*, trust-region-reflective algorithm).

Next, we identified the end of each HIS segment for trials revealing the within-trial skill drop by fitting a double-sigmoidal function $d(t)$ to the min–max normalized skill time series. This model comprised three components: a plateau skill level P, within-trial gain dynamics $G(t)$, and within-trial drop dynamics $D(t)$:

$$d(t) = P + G(t) + D(t) \tag{2}$$

where

$$\begin{aligned} P &= C_0 \\ G(t) &= C_1 \cdot \left(1 - e^{-\lambda_1(t-d_1)}\right) \\ D(t) &= -C_2 \cdot \left(1 - e^{-\lambda_2(t-d_2)}\right) \end{aligned} \tag{3}$$

Here, C_{0-2} controlled the magnitude of each component, λ_{1-2} the activation rate, and d_{1-2} the activation latency of the positive and negative sigmoidal functions. All parameters were constrained within the following bounds: $C_{0-2} \in [0,1]$, $\lambda_{1-2} \in [0,0.5]$, and $d_{1-2} \in [0,10000]$.

Parameter optimization was performed with 600 random initializations—300 single-sigmoid and 300 double-sigmoid fits (*lsqcurvefit.m*, trust-region-reflective algorithm). The parameter set, yielding the lowest Bayesian Information Criterion (BIC) was retained for further analysis, ensuring an optimal balance between model fit and complexity.

This modeling framework effectively isolated within-trial skill decay $D(t)$ from learning-related gains. The end of each HIS segment was defined as the time of maximal deceleration in $D(t)$ (i.e., the second derivative peak; **Fig 2C** and **Fig S2**). We then quantified HIS segment content (keypress #, keypress rates) changes within and across-individuals.

Chunking organization

To identify chunk boundaries within learned motor sequences, we applied hierarchical clustering to individual keypress transition times (KTTs) during HIS segments[93]. Chunk boundaries were defined as transitions longer in sequential context than those in non-sequential context, reflecting natural segmentation points in performance. Within each chunk, KTTs during sequential execution (KTT_{seq}) were equal to or shorter than those observed in a non-sequential context (KTT_{pairs}), consistent with previous reports of reduced transition times within well-learned chunks. To identify chunk boundaries within learned motor sequences, we applied hierarchical clustering to each keypress transition time (KTT) during HIS segments[93]. Chunk boundaries were defined as transitions longer in sequential

context than those in non-sequential context, reflecting natural segmentation points in performance. Within each chunk, KTTs during sequential execution (KTT_{seq}) were equal to or shorter than those observed in a non-sequential context (KTT_{pairs}), consistent with previous reports of reduced transition times within well-learned chunks[61-63].

Dendrogram was created using the within-individual, absolute KTT_{pairs}-corrected KTT_{seq} values to group temporally adjacent transitions (**Fig 3D** and **Fig S7**). The dendrogram was then cut at a threshold of zero, such that any KTT_{seq} longer than its corresponding KTT_{pair} defined a chunk boundary. We then quantified the number of chunks, average chunk content, and chunk rate within each HIS segment.

This approach, validated prior methods comparing transitional durations within and outside sequence contexts[61,64,65], reproduced established learning-related changes in chunk structure—specifically, a decrease in chunk number and a corresponding increase in chunk content across practice [46,94,95] (**Fig S10**).

MRI acquisition

Structural MRI scanning was performed on a 3T MRI scanner (GE Excite HDxt and Siemens Skyra) with a 32-channel head coil. High-resolution, T1-weighted anatomical images (1 mm^3 isotropic MPRAGE sequence) were acquired for each participant in Experiment 3 to allow surface-based cortical dipole estimation from MEG signals.

MEG acquisition

Continuous MEG was recorded at a sampling frequency of 600 Hz with a CTF 275 MEG system (CTF Systems, Inc., Canada) while participants were seated in an upright position. The system is composed of a whole head array of 275 radial 1st-order gradiometer / SQUID channels housed in a magnetically shielded room (Vacuumschmelze, Germany). Two of the gradiometers were malfunctioning and were not used. A third channel was removed (MLT16-1609) after visual inspection of the data indicated the presence of high noise levels for all recordings, resulting in 272 total channels of MEG data. Synthetic 3rd order gradient balancing was used to remove background noise. A TTL trigger was used to temporally align the behavioral and MEG data. Head position indicator points were monitored in the scanner coordinate space using head localization coils placed on the nasion, left and right pre-auricular locations of the participant's head. These coil positions were also recorded in the subject's T1-MRI coordinate space during the session using a stereotactic neuronavigation system (BrainSight, Rogue Research Inc.).

MRI data analysis

MRI data was analyzed using the FieldTrip[96], freesurfer[97] and Connectome Workbench[98]. Individual high-resolution T1 MRI was used to construct volume conduction models via

single-shell head corrected-sphere approach. Source models and surface labels from the HCP-MMP atlas[98] were created for each participant using inner-skull and pial layer surfaces.

MEG data analysis

MEG data was analyzed using the FieldTrip[96], EEGLAB[99] and SpectralEvents (https://github.com/jonescompneurolab/SpectralEvents) toolboxes, and custom analysis scripts developed in MATLAB 2023b.

Preprocessing

Raw MEG data were high-pass filtered at 0.1 Hz with fourth order non-causal Butterworth filter. Powerline noise (60 Hz) and its harmonics (120 Hz) were removed by spectrum interpolation implemented in Fieldtrip. Independent Component Analysis (ICA) was fitted using EEGLAB's implementation of InfoMax after pre-whitening with Principal Component Analysis (PCA) to retain 40 independent components. Spatial topographies and time series of all independent components were visually inspected and those determined to be strongly associated with known electrocardiogram, eye movements and blinks, and head movement artifacts were removed. MEG activity was then reconstructed using retained independent components and all principal components, which were not used for ICA analysis.

Source reconstruction and parcellation

Source reconstruction of MEG data was performed using the standard pipeline in Fieldtrip. Individual volume conduction model calculated from individual high-resolution T1 MRI was used to generate the forward solution at each source dipole location. The linearly-constrained minimum-variance (LCMV) beamformer was used to compute inverse-solution from sensor-space MEG activity. The individual inverse solution data covariance matrix was obtained by averaging the mean covariance matrices of practice and rest intervals. Specifically, sensor-space MEG covariance was calculated for each 10 second practice and rest interval and averaged over trials. The individual sample noise covariance matrix was computed from 6-mins of individual pre-training rest MEG data recorded during the same session. A total of 15,684 surface-based cortical dipoles were estimated. The individual HCP-MMP atlas model, which defines 180 parcellated cortical areas per hemisphere was used to extract source-space parcellated MEG activity by averaging activity within each cortical area.

Theta-gamma phase amplitude coupling

We measured the strength of PAC for a wide set of amplitude frequency ranges using the modulation index (MI) as introduced previously [100]. We first filtered (using pop_eegfiltnew.m from EEGLAB) continuous source-space parcellated MEG signal within the respective frequency bands of interest (θ=4-8Hz and γ=30-110Hz with a step of 5Hz and a window of ±6Hz). The frequency window of γ band was chosen such that it constituted twice the centre frequency of the phase signal. This procedure ensures that the side peaks that arise if the

amplitude signal is modulated by a lower-frequency phase signal are included [101]. We then extracted the instantaneous phase from the lower-frequency signal and the amplitude from the higher-frequency signal using the Hilbert transform.

During Experiment 3, subjects' HIS segments started at the beginning of each practice trial and finished 4.10±0.11 sec later (**Fig S10C**). Thus, we extracted the time window of [0, 4] sec (HIS segment) and [4, 10] sec (post-HIS segment) relative to practice trial onset. We additionally analyzed the time window of [4, 8] sec to control for the time window length between HIS and post-HIS segments (**Fig S12B**). Next, we concatenated the phase and amplitude signals for each practice trial and time window (18 phase bins) and computed the modulation index (MI) following established methods [102]. To standardize MI values across cortical areas, amplitude frequencies, and time windows, we generated 200 surrogate MIs by circularly shifting the theta-phase time series by a random interval greater than 600 samples (1s at the given sampling rate), producing a null distribution of MI values. A normal distribution was then fit to each surrogate set (*normfit.m*) to estimate its mean and standard deviation, which were used to z-transform the raw MI values. This normalization procedure controls for potential confounds related to amplitude power, phase properties, or evoked activity due to the transition from a rest to a practice interval that might otherwise introduce spurious differences in PAC[103]. The standardized MI values therefore permit valid comparisons across time windows and amplitude frequencies[101]. Cortical parcels exhibiting significant PAC were identified as those with normalized MI values significantly greater than zero (*t*-test, cluster-based permutation correction). Finally, θ/γ PAC values within each significant cluster were averaged for subsequent analyses.

Oscillatory bursting analysis

Spectral burst analysis was conducted in both sensor and source (parcellated) space MEG data, following previously established methods[104]. Transient high-power bursts were detected and characterized using the SpectralEvents Toolbox, which identifies *spectral events* as local maxima in time–frequency power exceeding a specified threshold. The analysis was event-overlap–agnostic, with the detection threshold set at six times the median power (6× factors-of-the-median, FOM) across time for each frequency bin[38]. Bursts were detected across 1–40 Hz in a 1-Hz step from continuous MEG recordings spanning the entire task period (from the start of the first to the end of the last practice trial). Each detected event was characterized by its peak time, power, central frequency, and duration (**Fig S14**). Event rate was defined as the number of detected bursts per second within HIS and post-HIS segments. Event duration was computed as the full-width at half-maximum (FWHM) of the power distribution in both the time and frequency domains, corresponding to the region where power exceeded half of the event's local maximum. Following the recommended procedure used in the previous studies[104] the first 1 s of each practice interval was excluded from analysis to minimize contamination from transient spectral activity associated with practice onset.

STATISTICAL ANALYSIS

We assessed the significance of several variables during the HIS segment, including the number of keypresses, keypress rate, number of chunks, chunk rate, chunk content and HIS duration. We compared these metrics across different groups and as practice progressed within each skill group. To perform the across-group comparison, we used a one-way ANOVA (*anova1.m*) followed by Tukey's honestly significant difference procedure for post-hoc analysis (*multcompare.m*). The progression of these values with practice trials was evaluated using linear-mixed effects models (LMM, *fitlme.m*). The choice of an LMM was made to accommodate inter-individual differences by including them as a random effect. All models were fitted using restricted maximum likelihood estimation. We tested the significance of fixed effects in the model using a Type III analysis of variance (ANOVA) with Satterthwaite's method (*fixedEffects.m* and *anova.m*). For behavioral evaluations, we used trial number as the dependent variable to measure trial-by-trial development of variables in HIS segments. On the other hand, within-cluster averaged θ/γ PAC was the dependent variable when predicting the number of HIS contents (**Fig 5D**).

During the MEG analysis, we used a cluster-based multiple comparison correction approach to identify frequencies of interest, spatial contribution of parcellated brain regions to θ/γ PAC and β bursts[105]. This correction approach was chosen to address the multiple comparisons problem inherent in the high spatial resolution of the HCP-MMP atlas, while effectively leveraging its specific parcellation of 360 cortical brain regions.

Figures

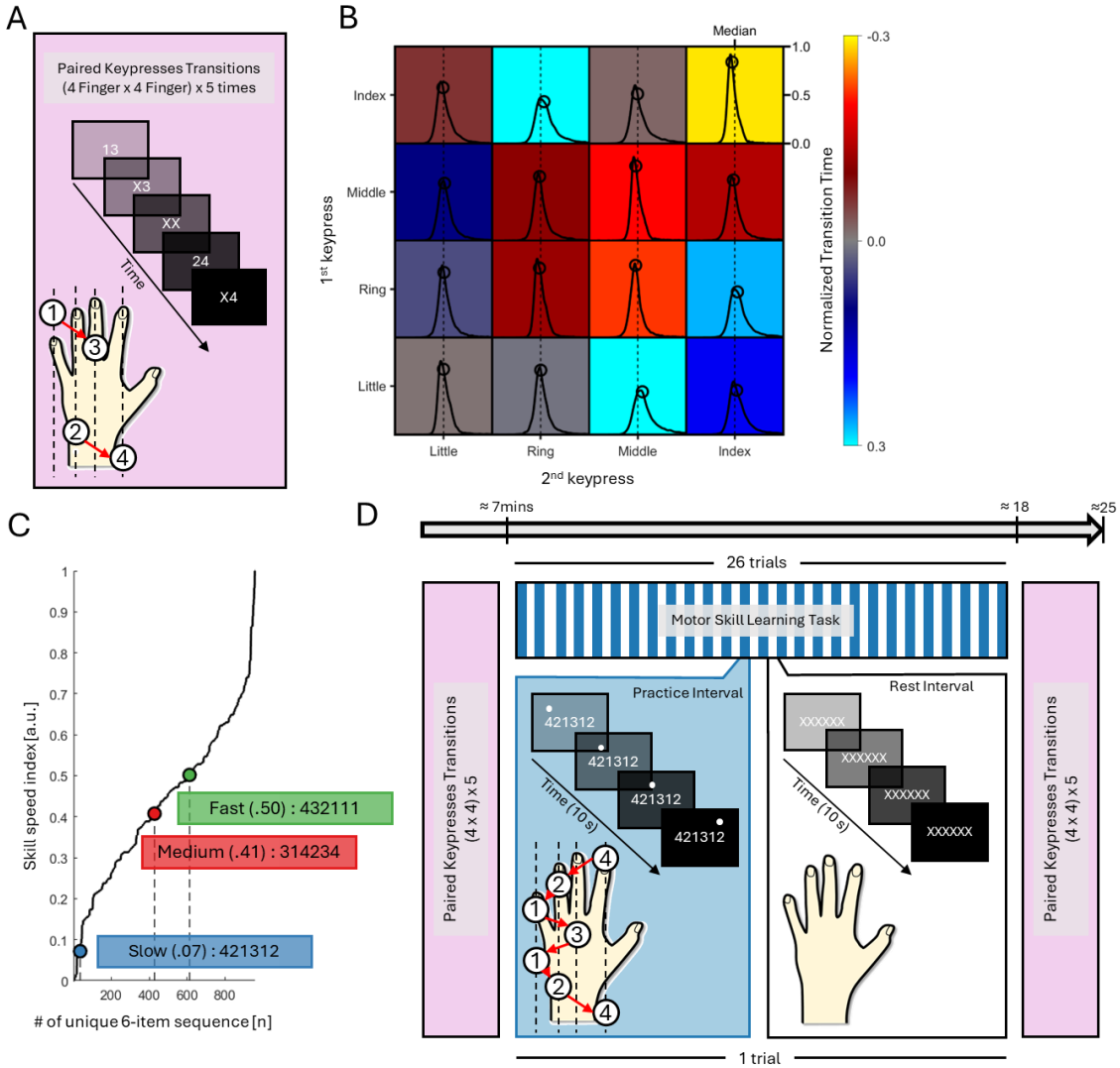

Figure 1. Experimental Design.

A, **B** and **C**. **Naturalistic skill speed index (Experiment 1).** **(A)** Healthy volunteers (N=2,152) typed all possible 16 keypress pairs in pseudo-random order five times each as fast and accurately as possible with four fingers (little, ring, middle and index) of the left non-dominant hand**. (B)** Within-subject z-normalized keypress transition times (KTT_{pairs}) were calculated and then concatenated across all participants resulting in a 4x4 KTT_{pairs} matrix superset (reflecting the speed of keypress pair transition times typed in a non-sequential skill context). Color-coding depicts the median z-score shifts for each KTT_{pairs} superset. Black lines depict the distribution of normalized KTT_{pairs} with the median indicated by a circle. The dashed vertical black line corresponds to the median across all 4x4 KTT_{pairs} (z-score=0). Yellow and light blue denote faster and slower transitions, respectively, relative to the

overall median. **(C)** We then used these KTT_{pairs} to compute a naturalistic skill speed index across all 960 possible 6-item sequences (x-axis), where each sequence's duration was scaled between 0 and 1 to indicate its relative speed (y-axis). **(D) Learning dynamics of three different skills (Experiment 2).** We selected three skill sequences along this range: fast (SSI=0.50), medium (SSI=0.41) and slow (SSI=0.07). Participants (N=407) **w**ere randomly assigned to train one of the three skills (slow, medium, or fast) and instructed to perform the task as fast and accurately as possible following an experimental paradigm previously described[19]. Each trial consisted of 10 s of practice interleaved with 10 s of rest for a total of 26 trials[55]. Prior to and after training, participants also completed the pseudo-randomized task described in Experiment 1 to compare within-subject skill sequence-embedded KTTs (KTT_{seq}) and those executed in a non-sequential context (KTT_{pairs}).

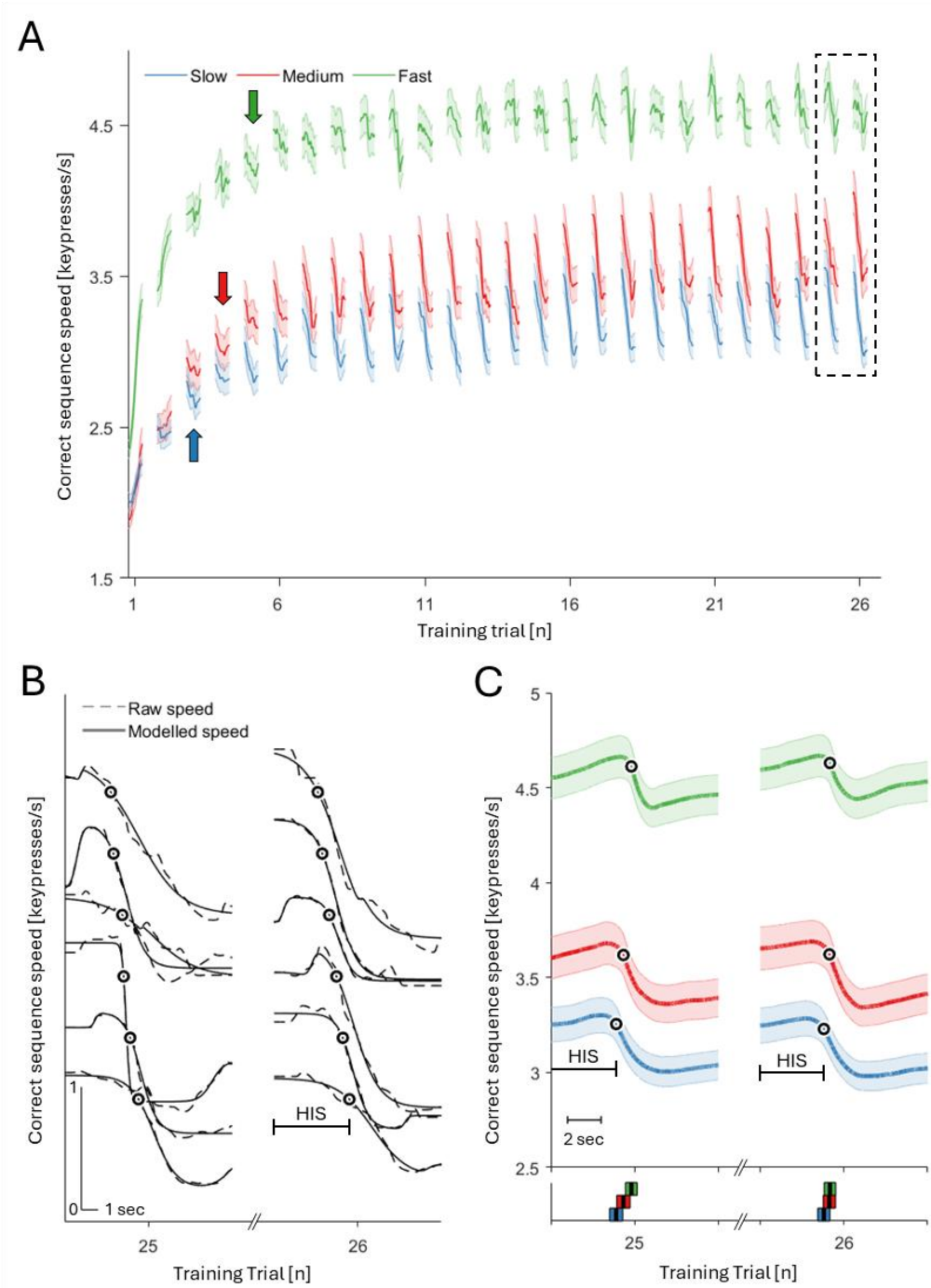

Figure 2. Segments of high initial skill (HIS) emerged with practice across skills.

(A) Group-level performance curves (correct sequence speed [keypresses/sec][77] , mean±sem) in participants learning slow (blue, N=122), medium (red, N=127) and fast (green, N=158) sequential skills. Across the three groups, rapid early gains in performance give way to a near-plateau skill level. Arrows indicate the first practice trial in which within-trial skill drops emerge, with these dynamics persisting across subsequent trials to the end

of the session. **(B)** Next, we fit a double-sigmoid function to model individual practice trial performances (**Fig S2**). Examples of raw (dotted lines) and modelled (solid lines) single practice trials 25 and 26 (box in **Fig 2A**). Note the high initial skill (HIS) segments, points of maximum deceleration (circles) and following sharp performance declines. **(C)** Group level HIS segment dynamics (trials 25 and 26)**.** Within each skill group, subjects' models were aligned to the end of the HIS segment and averaged. Bottom shows mean and 95% confidence intervals of the end of HIS segment for each group (**Fig S4C**).

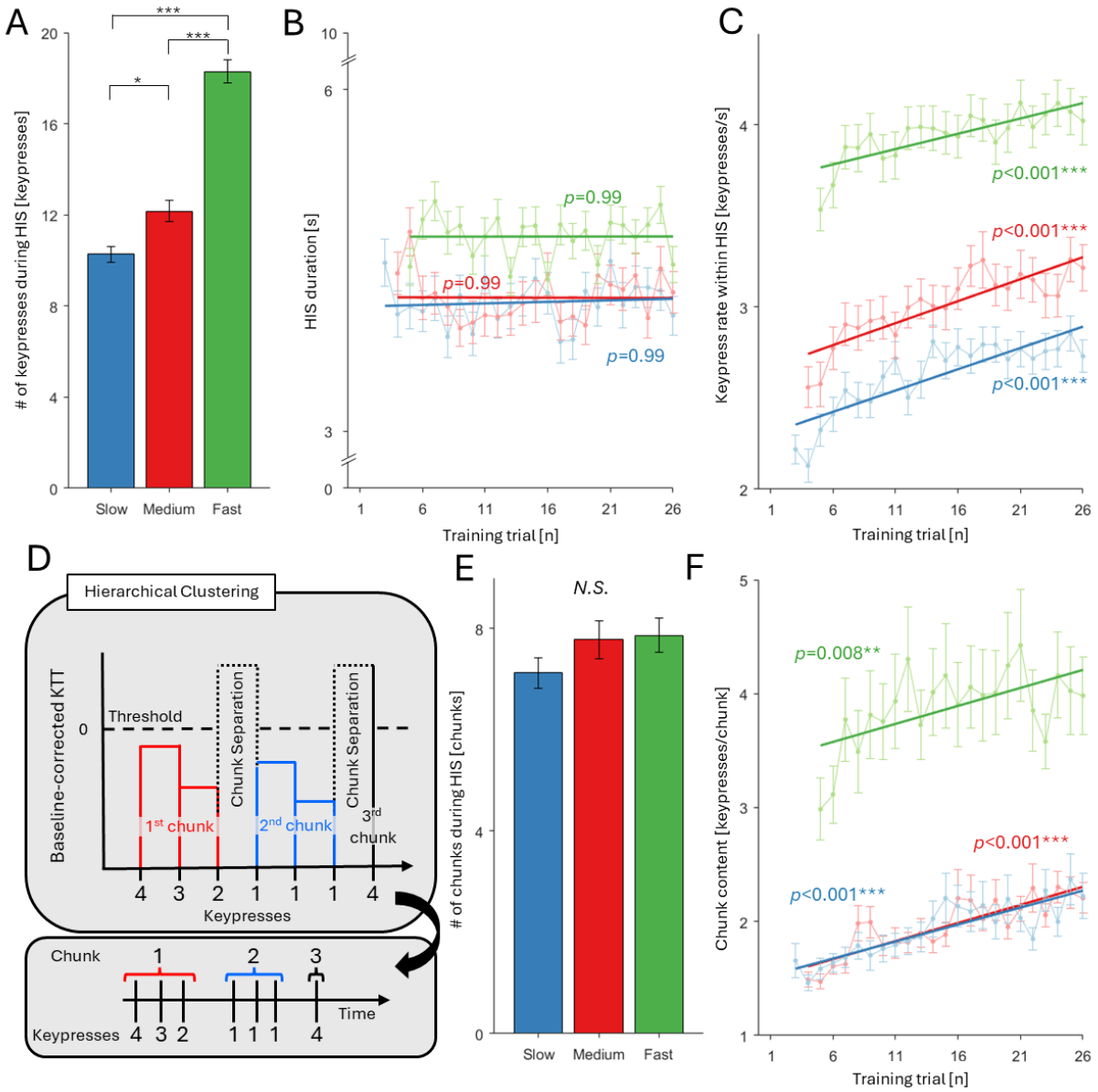

Figure 3. HIS segment keypress content increased with practice.

(A) HIS segment keypress content ranged between 10 and 18 keypresses (10.83±0.32, 12.63±0.46 and 18.86±0.51 keypresses/HIS segment learning the slow, medium and fast skills respectively) and increased with skill speed. Asterisks indicate statistically significant differences during post-hoc comparisons (*p < 0.05, **p < 0.01, ***p < 0.001). **(B)** HIS segment duration was not modified by practice (mean±sem; linear-mixed effects models [LMM], BHFDR corrected) and was longer for fast than for slow skills (**Fig S4A**). **(C)** Keypress rates during HIS segments increased progressively with practice in all skill groups (keypresses/s, mean±sem; LMM, BHFDR corrected). Asterisks indicate statistically significant increase in keypress rate with training (*p < 0.05, **p < 0.01, ***p < 0.001). Solid

lines show the linear-fitted model for each group. **(D)** Hierarchical clustering was implemented on the within-individual absolute KTT_{pairs} corrected KTT_{seq} (**Methods**). The threshold to determine the separation between clusters (chunks) was set to 0 (KTT_{seq} longer than KTT_{pairs}; **Fig S3**). **(E)**. The mean number of chunks within HIS segments ranged between 7 and 8 for all skills (Slow: 7.13±0,30, Medium: 7.78±0.37, and Fast: 7.87±0.34 chunks/HIS segment; one-way ANOVA, p=0.27), reminiscent of the "rule of 7" [14-17]. **(F)** Chunk content (keypresses/chunk) increased progressively with practice in all skill groups. Solid lines show the linear-fitted model for each group (LMM, BHFDR corrected). Asterisks indicate statistically significant increase in chunk content with training (*p < 0.05, **p < 0.01, ***p < 0.001).

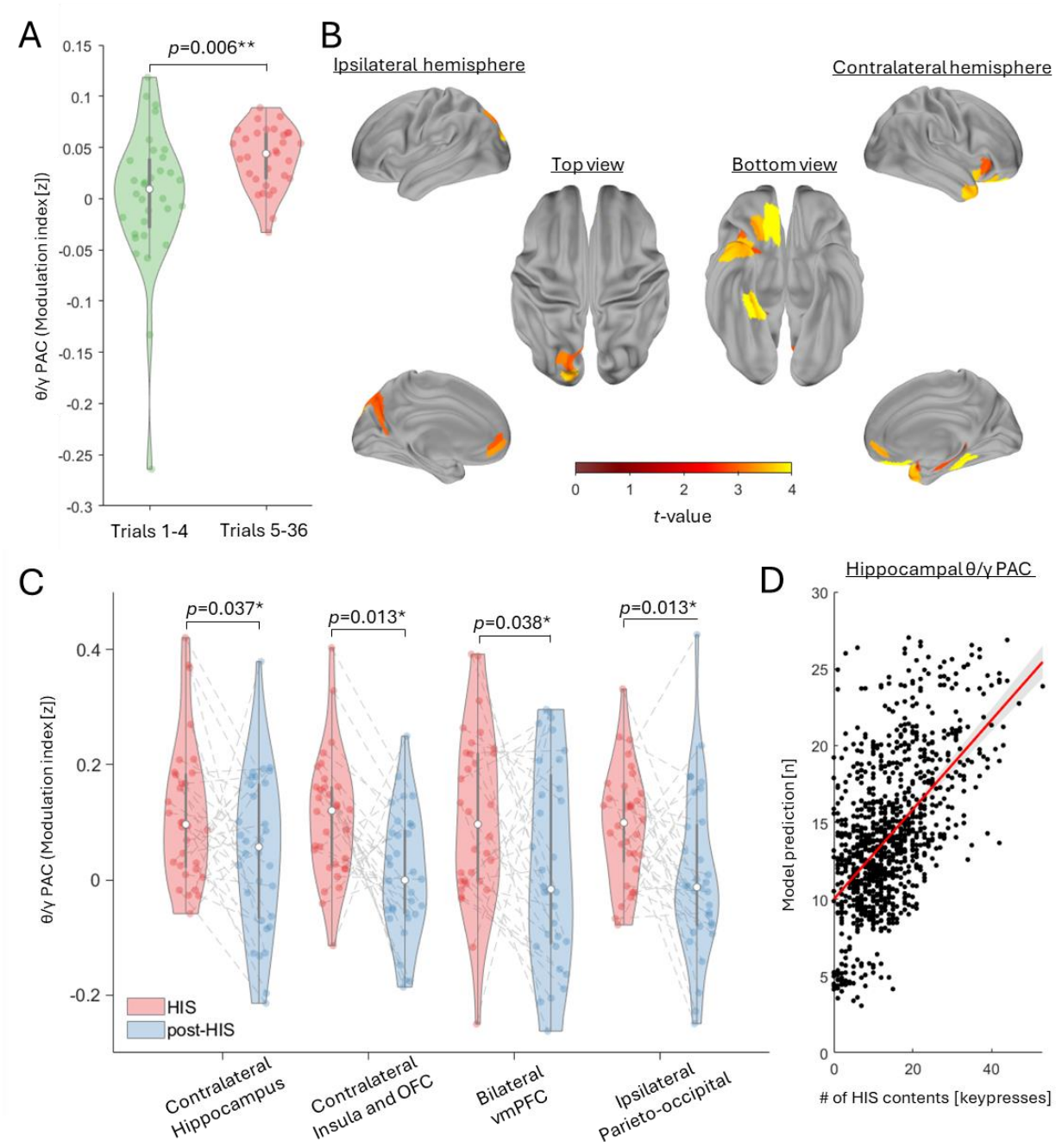

Figure 4. θ/γ PAC predicted HIS segment content and overall skill.

(A) Whole-brain source-space parcellated MEG θ/γ PAC was significantly higher during HIS segments (trials 5-36) than in the same time window of trials preceding the appearance of HIS segments (trials 1-4). **(B)** During HIS segments (trials 5-36), θ/γ PAC strength was significantly higher in contralateral hippocampus, insula and orbitofrontal cortex (OFC), bilateral ventromedial prefrontal cortex (vmPFC), and ipsilateral parieto-occipital regions (relative to time-shifted 200 surrogates[103]; cluster-forming threshold t>2.74 and

distance<20mm, number of permutation=2,000, $p<0.01$, **Table S1**). **(C)** θ/γ PAC during HIS segments (0-4sec) was significantly higher than following HIS segments (4-10sec) in all regions identified in **B** (paired *t*-test, BFDR corrected; **Fig S12B**). **(D)** Out of these regions, only hippocampal θ/γ PAC predicted HIS segment content (number of keypresses/HIS segment; LMM, $F_{986}=13.5$, $t_{986}=3.68$, $p=9.89\times10^{-4}$, $R^2=0.28$, see **Fig S13** for other regions) as well as overall skill (**Fig S15B**).

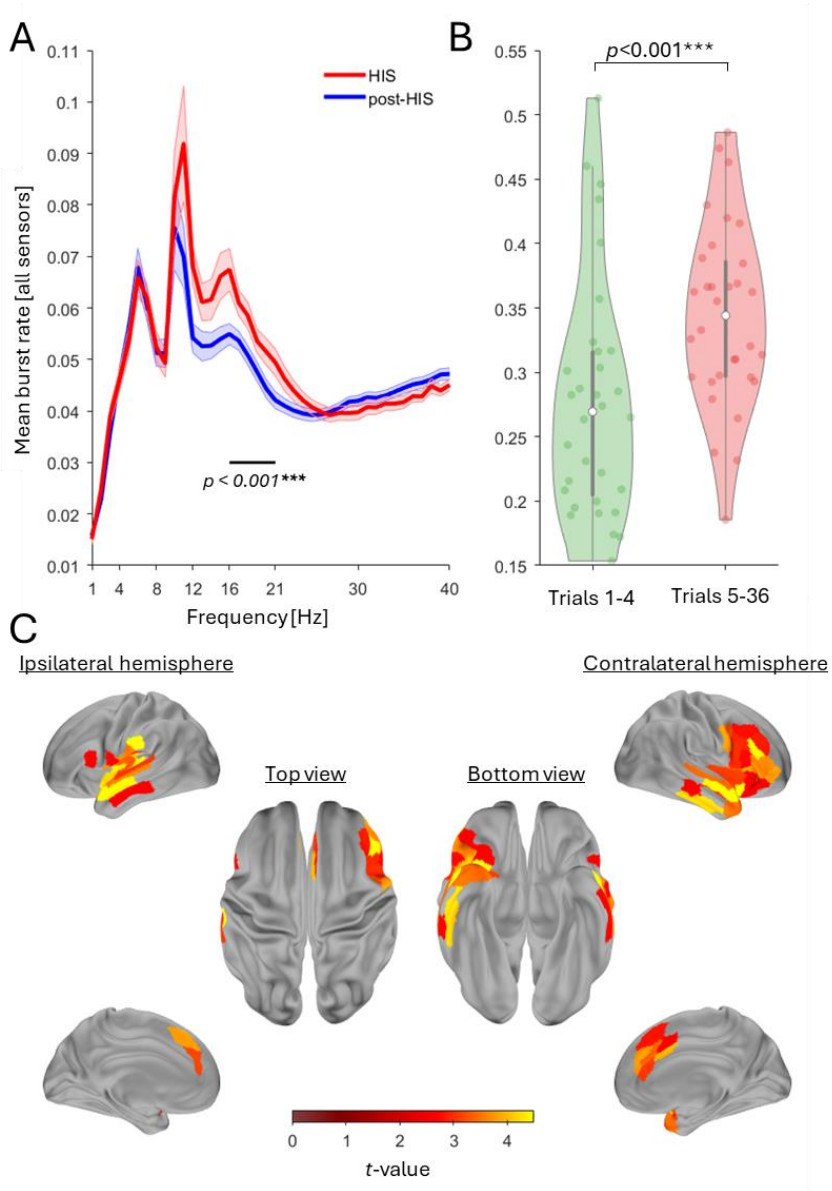

Figure 5. Increased beta burst activity in the bilateral insula, and frontal, temporal and anterior cingulate cortices linked to HIS segments.

(A) Broad-band whole-brain sensor-space MEG oscillatory burst rates[38] during HIS- and post-HIS segments (trial 5-36; HIS segment was determined in each trial and each participant). Note the significantly higher burst activity in the 16-21 Hz range during HIS relative to the post-HIS segments (cluster-forming threshold $t>3.37$, number of permutations=2,000, $p<0.01$). β band bursts during HIS segments displayed higher power, higher frequency, and longer duration compared to bursts observed following HIS segments (**Fig S14**) **(B)** β burst rate activity was significantly higher for the same 0-4sec time window, in trials with HIS (5-36) than in those preceding the appearance of HIS segments (1-4) (paired *t*-test, $t_{31}=-3.71$, $p<0.001$). **(C)** Bilateral insula and frontal, temporal and anterior cingulate

cortices were the main contributing regions to the higher source-space parcellated MEG β burst activity during HIS segments (cluster-forming threshold t>3.37 and distance<20mm, number of permutations = 2,000, $p<0.01$, **Table S2**).

Supplementary Figures

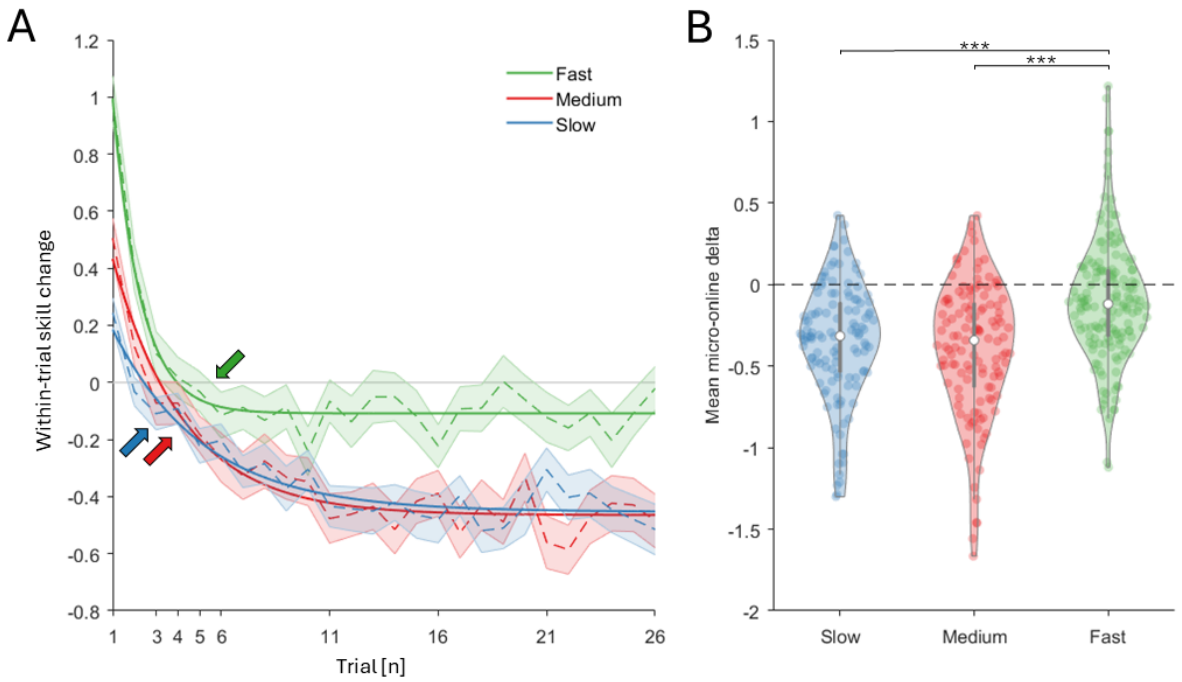

Figure S1: (A) Raw (dashed lines) and modelled (exponential function, solid lines) within-trial skill changes as a function of practice (Exp 2; mean±sem.). Note the initial within-trial skill gains (above 0 dashed line) followed by within-trial skill drops (below 0 dashed line, arrows denote the first practice trial at which skill drops emerge). **(B)** The magnitude of skill drops following HIS segments was larger in the slow and medium than in the fast skill group (trial 5-26, one-way ANOVA, $F_{2,404}$=21.2, p=1.82×10^{-9}). Asterisks indicate statistically significant differences during post-hoc comparisons (*p < 0.05, **p < 0.01, ***p < 0.001).

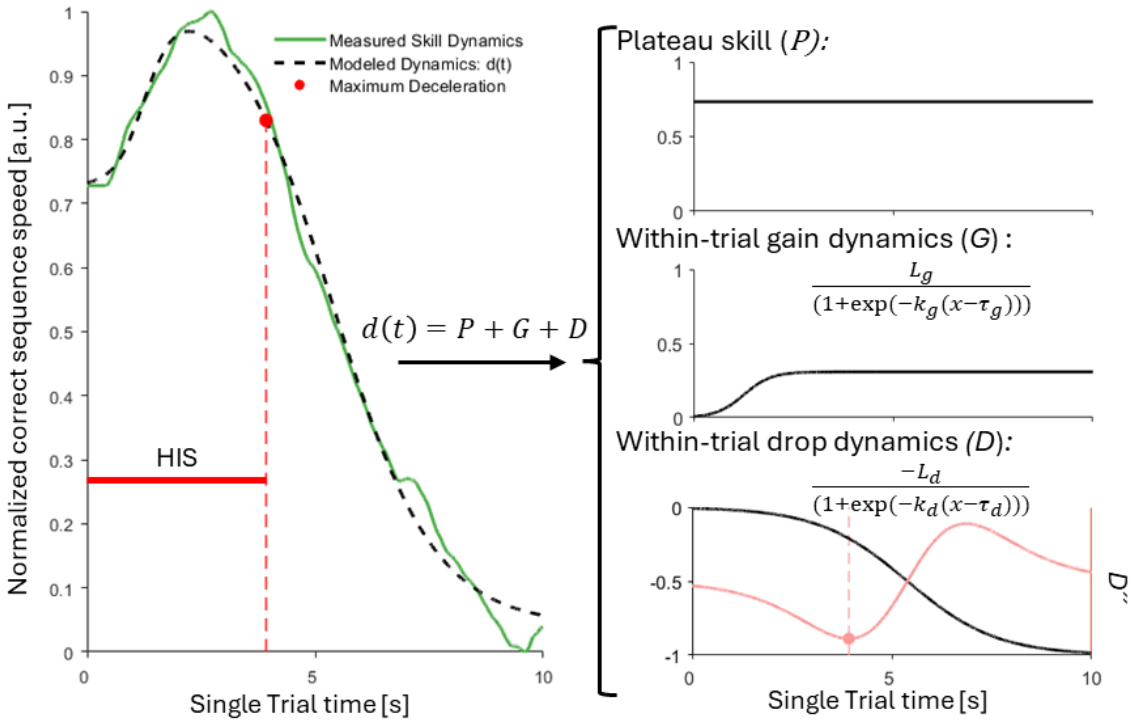

Figure S2: Modelling within-trial skill dynamics. Skill dynamics was modeled by fitting a double-sigmoidal function that includes plateau skill (*P*), within-trial gain (G) and within-trial drop (*D*) dynamics. The end of the HIS segment was defined by the maximum deceleration point of the within-trial drop dynamics (2nd derivative).

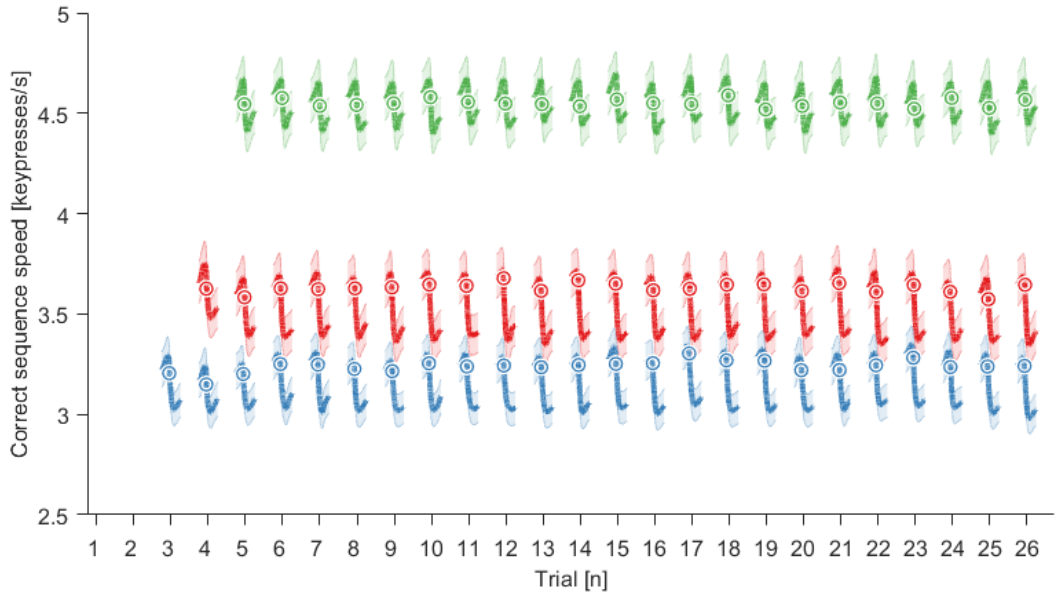

Figure S3: Group level within-trial HIS segment dynamics. Within each skill group, subjects' individual trial models were aligned to the end of the HIS segments and averaged (as shown for the last two trials in **Fig 2C**). Note the stability of this pattern following the emergence of HIS segments (trials 3, 4 and 5 for slow, medium and fast skills respectively).

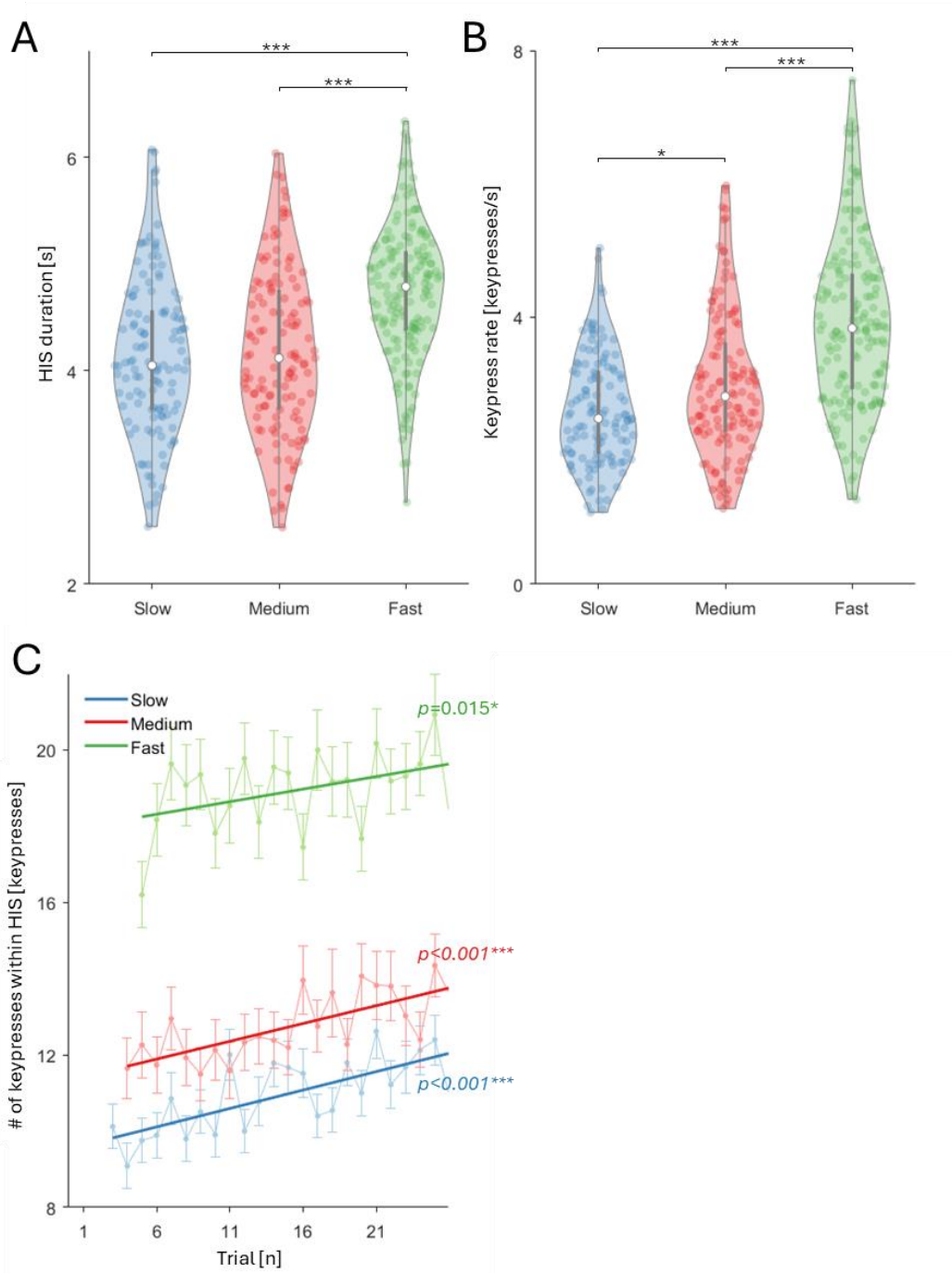

Figure S4: HIS characterization. Note **(A)** the longer mean HIS segment duration learning the fastest skill (one-way ANOVA, $F_{2,404}$=30.5, p=4.54×10^{-13}), **(B)** that keypress rates increased progressively with skill speed, and **(C)** that HIS segment keypress content increased progressively with practice in all skill groups.

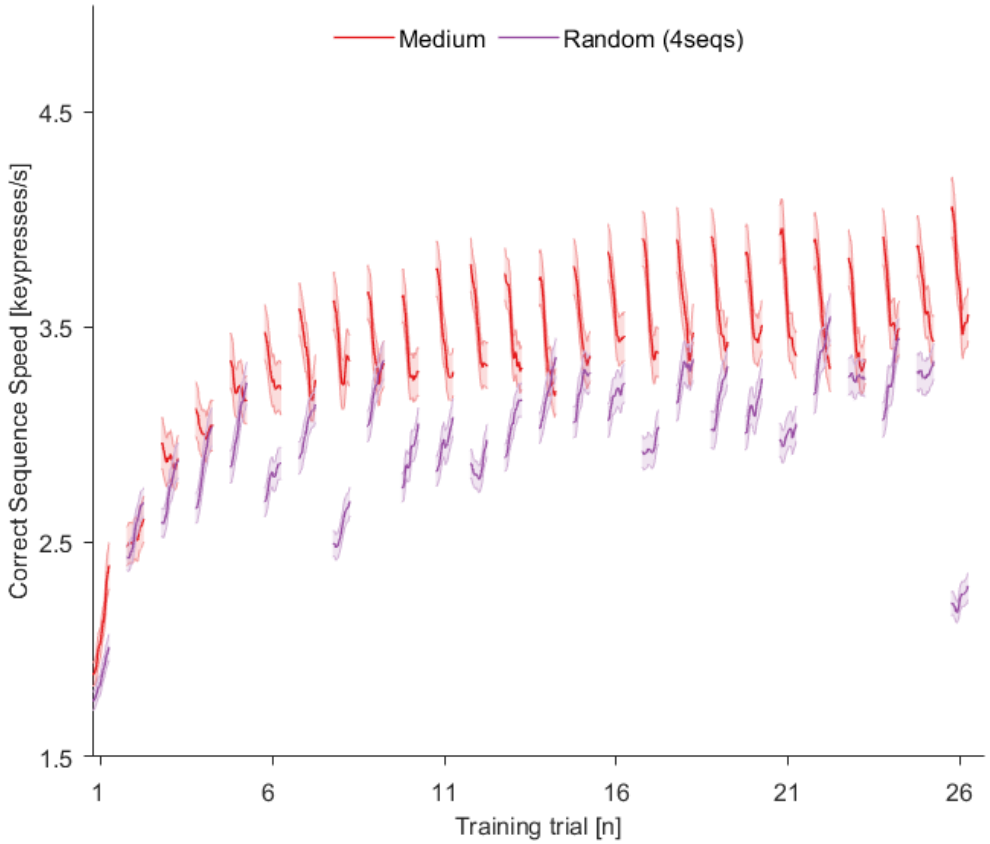

Figure S5: Practicing non-repeating sequences of comparable speed did not elicit HIS segments nor substantial learning. We have collected an additional group in which participants (N=156) practiced four non-repeating sequences in a pseudo-randomized order between trial 2 and 25 (mean±sem). In the first and last trials, participants trained the repeating medium skill sequence, enabling comparison of the beneficial effects of practicing repeating vs non-repeating skills on learning. Note that in contrast to their relatively comparable speed, practicing non-repeating sequences, (a) elicited as expected negligible learning in medium skill (first and last purple trials, compared with learning in the red trials) and crucially (b) HIS segment did not emerge. Thus, practice of non-repetitive tasks of relatively comparable speed elicited completely different within-trial skill dynamics that did not elicit HIS segments. These findings are inconsistent with speed-related fatigue originating HIS segment dynamics.

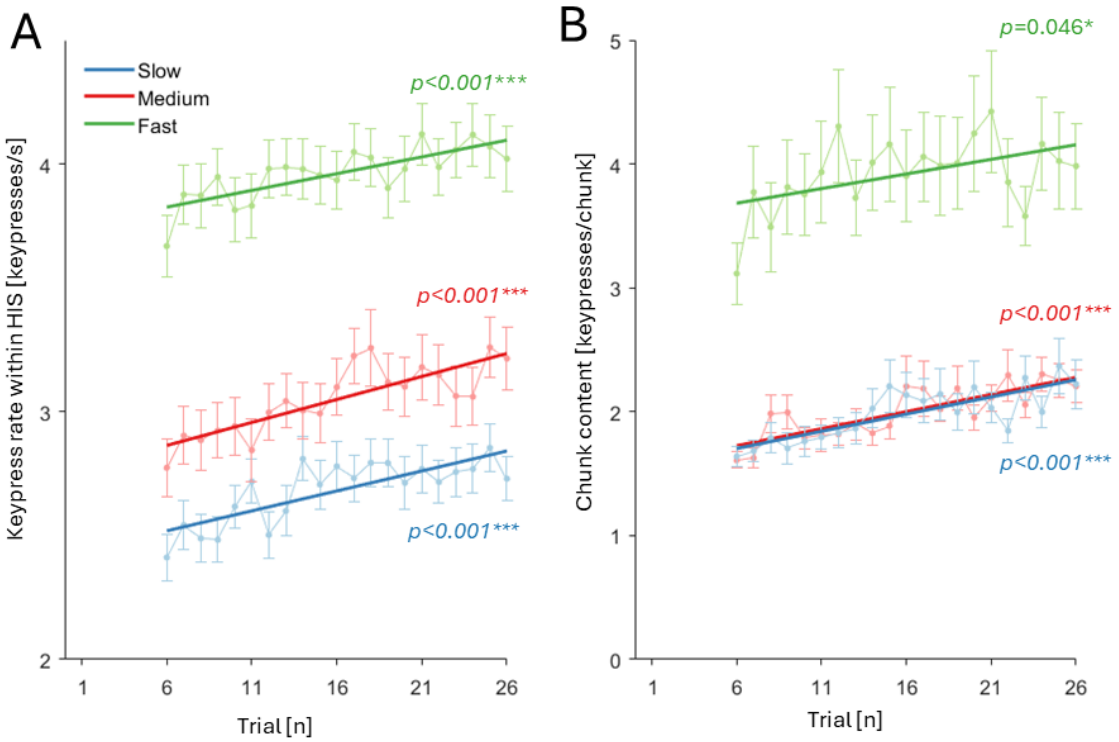

Figure S6: Restricting the analysis of HIS segment content to practice trials that follow rapid initial early learning (plateau period, trials 6-26) revealed that in spite of no substantial additional skill gains, **(A)** increase in keypress rates within HIS segments (trial 6-26, LMM, BHFDR corrected, Slow: $F_{1,2291}$=45.2, t_{2291}=6.73, p=3.28×10^{-11}, Medium: $F_{1,2430}$=58.4, t_{2430}=7.64, p=9.04×10^{-14}, Fast: $F_{1,3044}$=24.4, t_{3044}=4.94, p=8.42×10^{-7}) and **(B)** chunk keypress content increased with training in all skill groups (trial 6-26, LMM, Slow: $F_{1,2292}$=39.2, t_{2292}=6.26, p=6.90×10^{-10}, Medium: $F_{1,2432}$=45.7, t_{2432}=6.76, p=5.16×10^{-11}, Fast: $F_{1,3045}$=3.98, t_{3045}=2.00, p=0.046). Thus, HIS segment content continued to expand with training across groups, in the absence of substantial additional skill improvements.

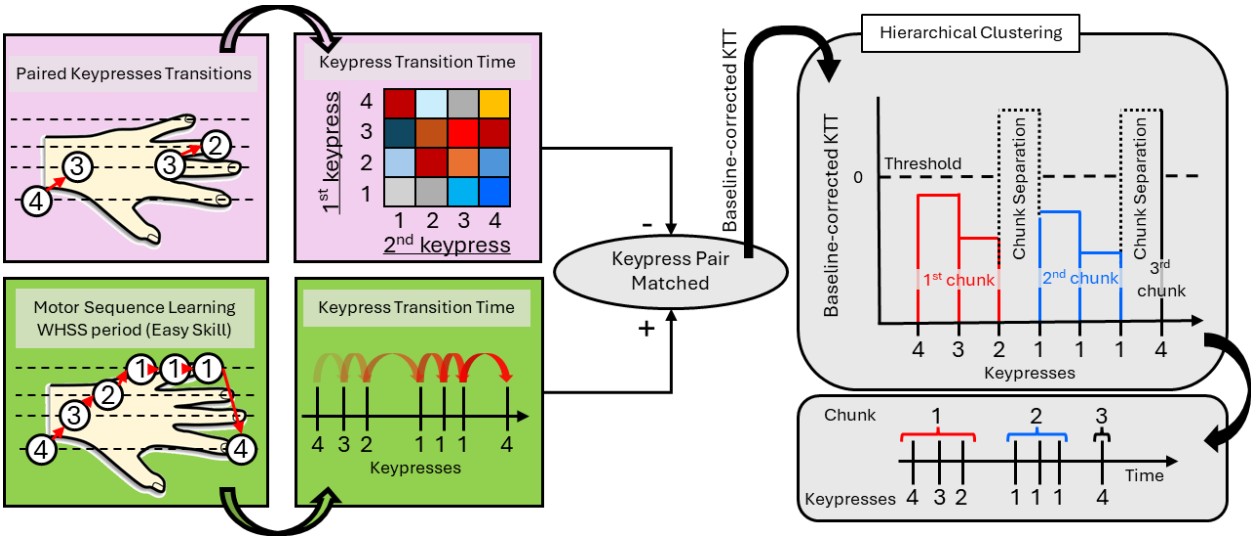

Figure S7: Hierarchical clustering of the pair-matched baseline corrected keypress transition times during the sequence learning tasks was used to unveil organization of keypress HIS content into chunks. Within-individual baseline KTT_{pairs} was determined by calculating the mean transition times collected before and after the skill learning task. Next, measurements of KTT obtained in the context of learning sequences (KTT_{seq}) were compared to those measured in a non-learning context preceding and following training in each individual (KTT_{pairs}). KTT_{seq} longer than KTT_{pairs} identified chunk boundaries. This analysis allowed us to quantify HIS content (number of chunks/HIS segment) as well as chunk content (keypresses/chunk).

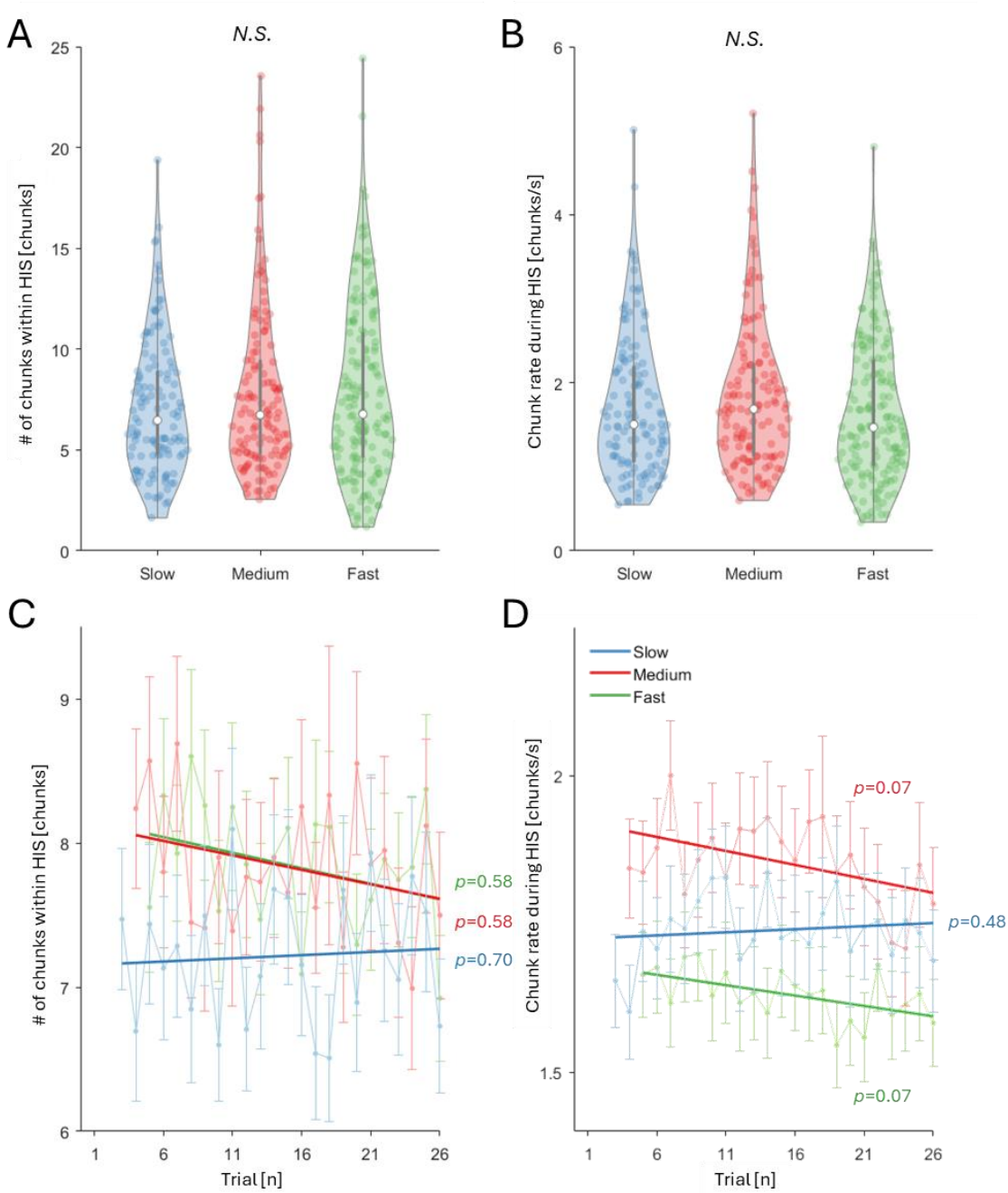

Figure S8: (A) The mean number of chunks/HIS segment and **(B)** chunk rate (chunks/sec) were comparable across skill groups (number of chunks, one-way ANOVA, $F_{2,404}$=1.33, p=0.27; chunk rate, $F_{2,404}$=2.06, p=0.13). **(C, D)** The overall chunk number nor the chunk rate (chunks/sec) during HIS segments did not change significantly in the course of training for any skill group (mean±sem, LMM, BHFDR corrected). Straight lines show the linear-fitted model for each group.

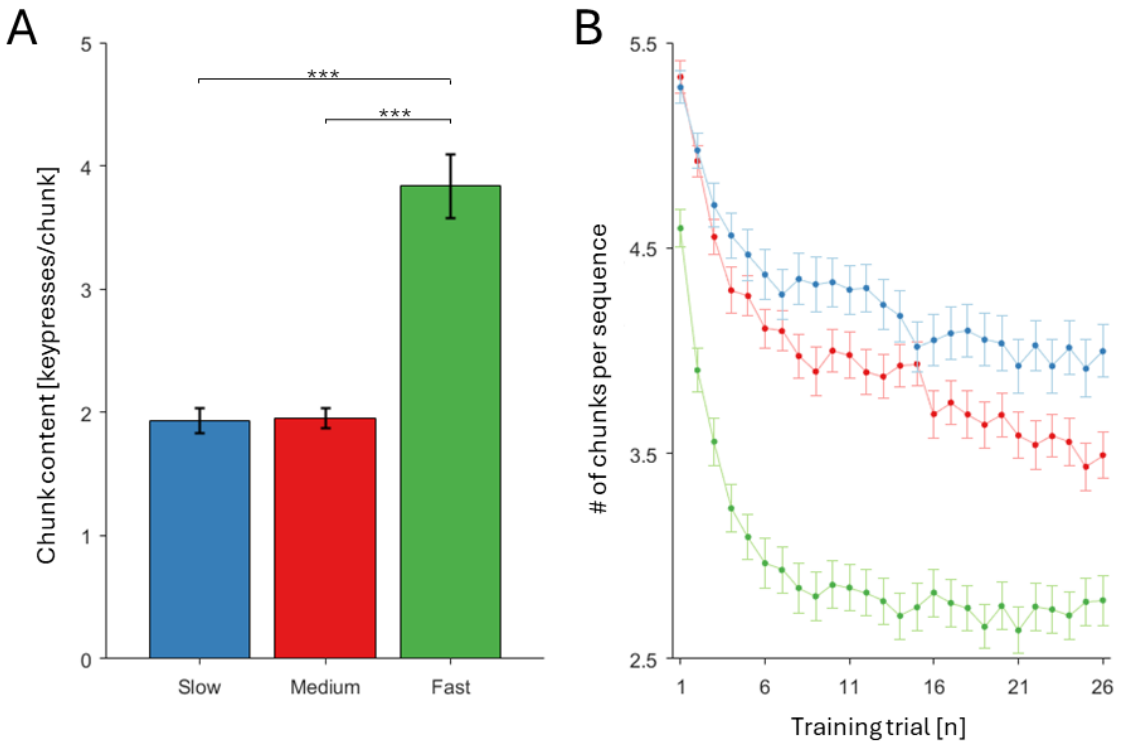

Figure S9: (A) The mean chunk content (keypresses/chunk, mean±sem.) within HIS segments was significantly larger practicing the fast skill than practicing the medium and slow skills (one-way ANOVA, $F_{2,404}$=36.5, p=2.61×10^{-15}). **(B)** Consistent with previous work[106], training resulted in a progressive reduction in the number of chunks/sequence.

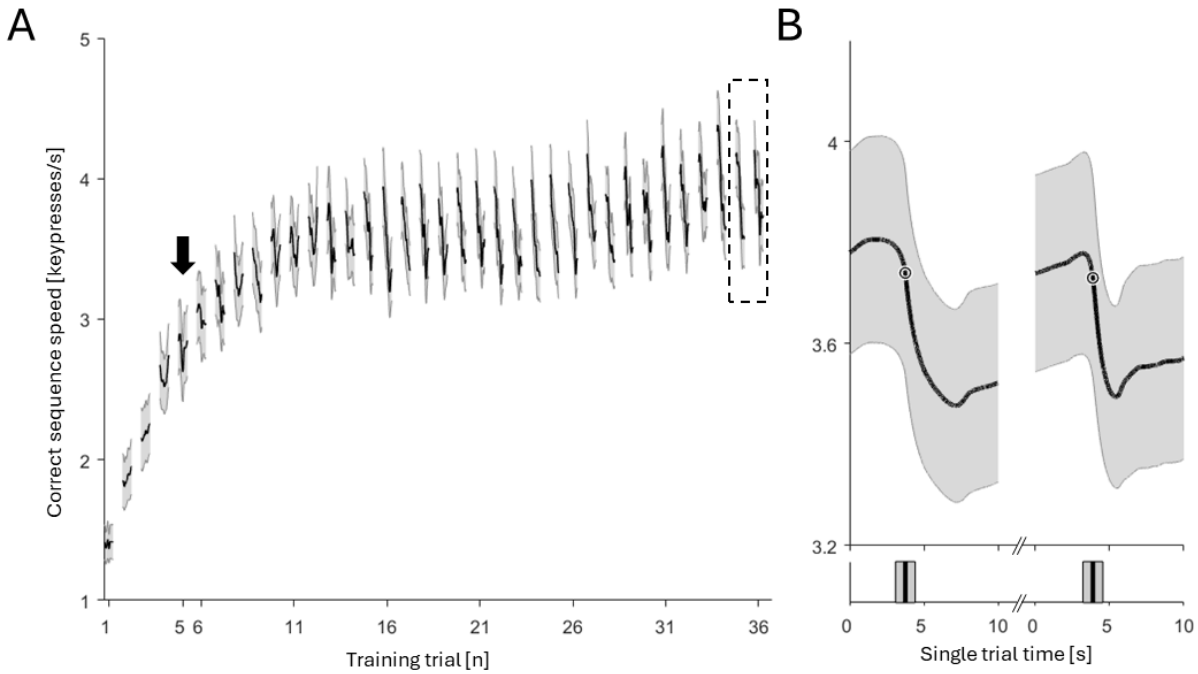

Figure S10: In Experiment 3, we evaluated MEG brain oscillatory dynamics in a dataset of subjects learning a medium speed sequential skill task over 36 practice trials (https://openneuro.org/datasets/ds006502/versions/1.0.0). **(A)** Performance curves in these participants (N=32) learning a medium sequential skill measured in the same way as in Experiment 2. The arrow denotes the emergence of HIS segment dynamics (trial 5), akin to those identified in Experiment 2 (**Fig 2A**). **(B)** Examples of group level skill dynamics on the last two trials (35 and 36, Experiment 3) aligned to the end of the HIS segment and averaged as described in Experiment 2. Thus, intra-trial dynamics described in Experiment 2 (**Fig 2**) were reproduced in a different data set in Experiment 3 practicing a medium speed skill.

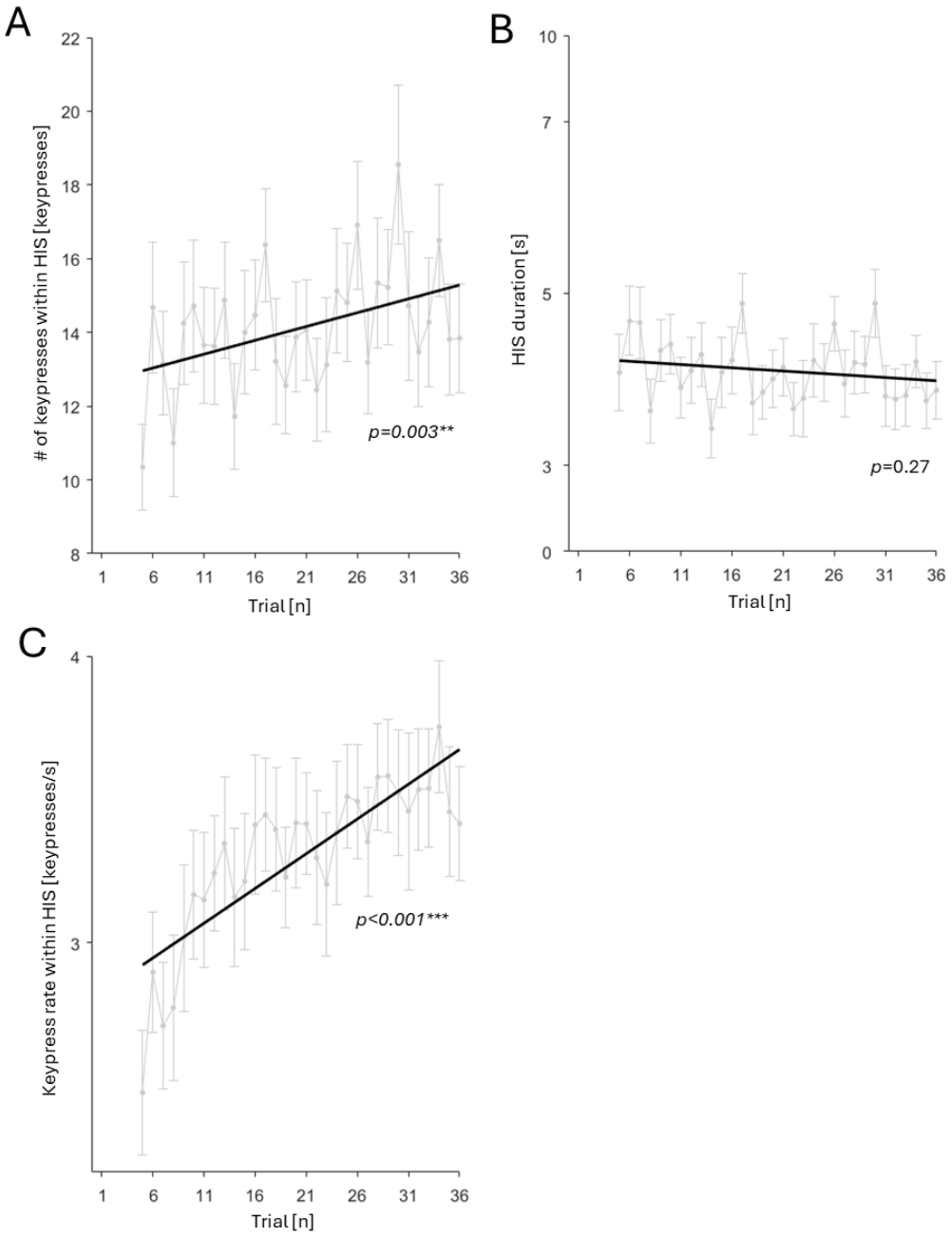

Figure S11: HIS segment characterization in Experiment 3. Practice resulted in **(A)** a progressive increase in keypress #/HIS segment identified in each training trial for each participant (mean±sem; LMM, $F_{1,985}$=9.00, t_{985}=3.0, p=3.0x10^{-3}, solid line shows the linear-fitted model), **(B)** stable HIS segments duration (LMM, $F_{1,1020}$=1.21, t_{1020}=-1.10, p=0.27), and **(C)** progressive increase in keypress rates during HIS segments (keypresses/s, mean±sem; $F_{1,985}$=104.2, t_{985}=10.21, p=2.5×10^{-23}). Thus, the reported training-dependent expansion of HIS segment content in Experiment 2 was reproducible across experiments in Experiment 3.

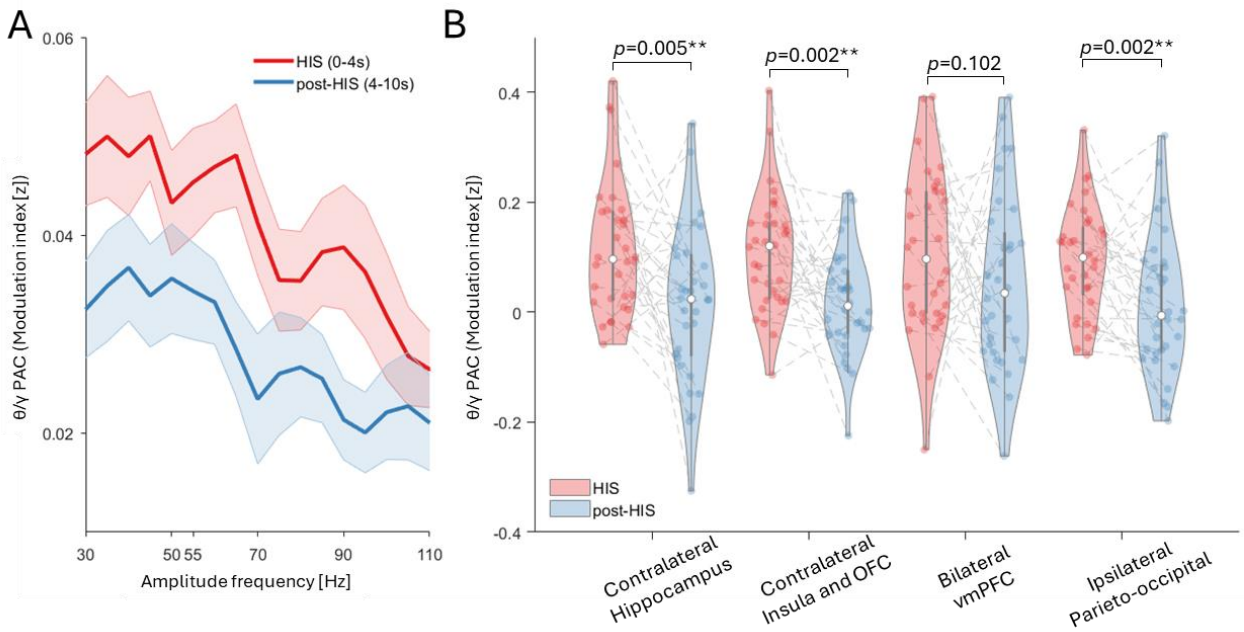

Figure S12: (A) Whole-brain source-space parcellated MEG θ/γ PAC strength normalized by 200 time-shifted surrogates during HIS and post-HIS segments (mean±sem., θ=4-8Hz and γ=30-110Hz with a step of 5Hz and a window of ±6Hz, mean±sem, trials 5-36). Given the stronger θ/γ PAC in the range of 30-55, we used this amplitude frequency range for further analyses. **(B)** Comparison of θ/γ PAC during HIS segments (0-4sec) with θ/γ PAC during an identical time window length immediately following HIS segments (4-8 sec) rendered a result similar to that in Fig 4C, which used a slightly longer time window following HIS segment (4-10s).

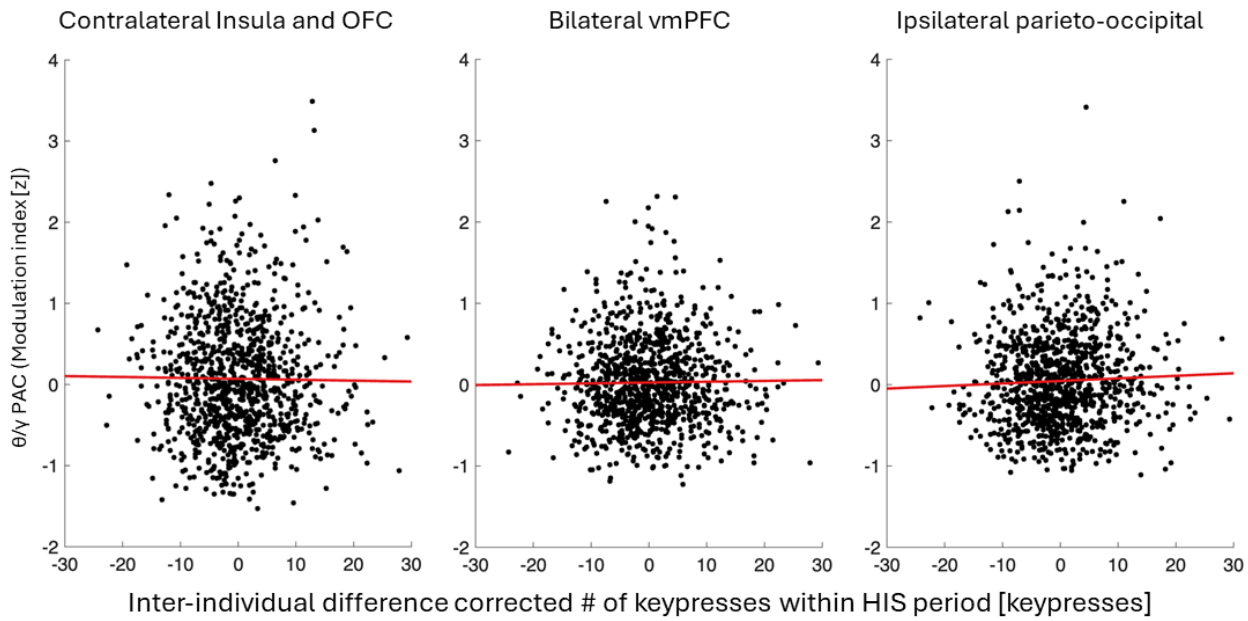

Figure S13: None of the regions shown in **Fig 4D**, other than the hippocampus showed a relationship between θ/γ PAC and HIS segment content (Contralateral insula and OFC: t_{986}=1.29, p=0.39, Bilateral vmPFC: t_{985}=-0.36, p=0.72, Ipsilateral parieto-occipital: t_{987}=0.44, p=0.72).

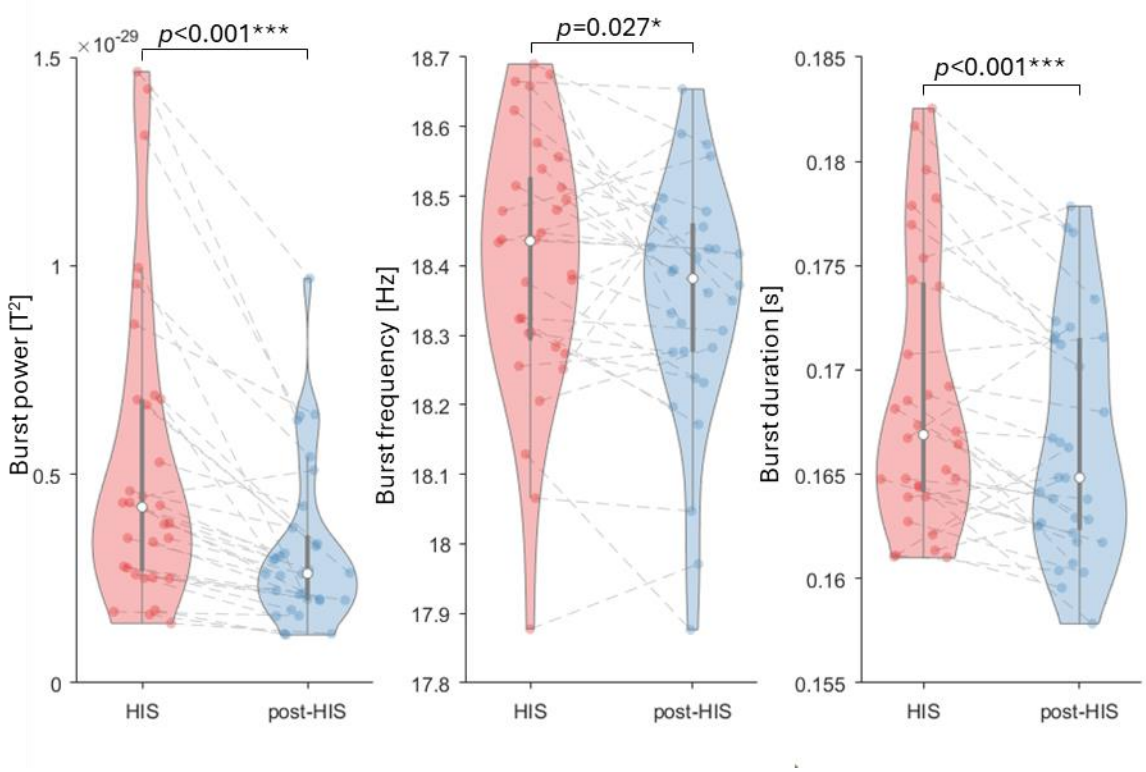

Figure S14: β band burst activity during HIS segments exhibited higher power, higher frequency, and longer duration than during post-HIS segments (paired t-tests). HIS segments were determined in each practice trial and each participant.

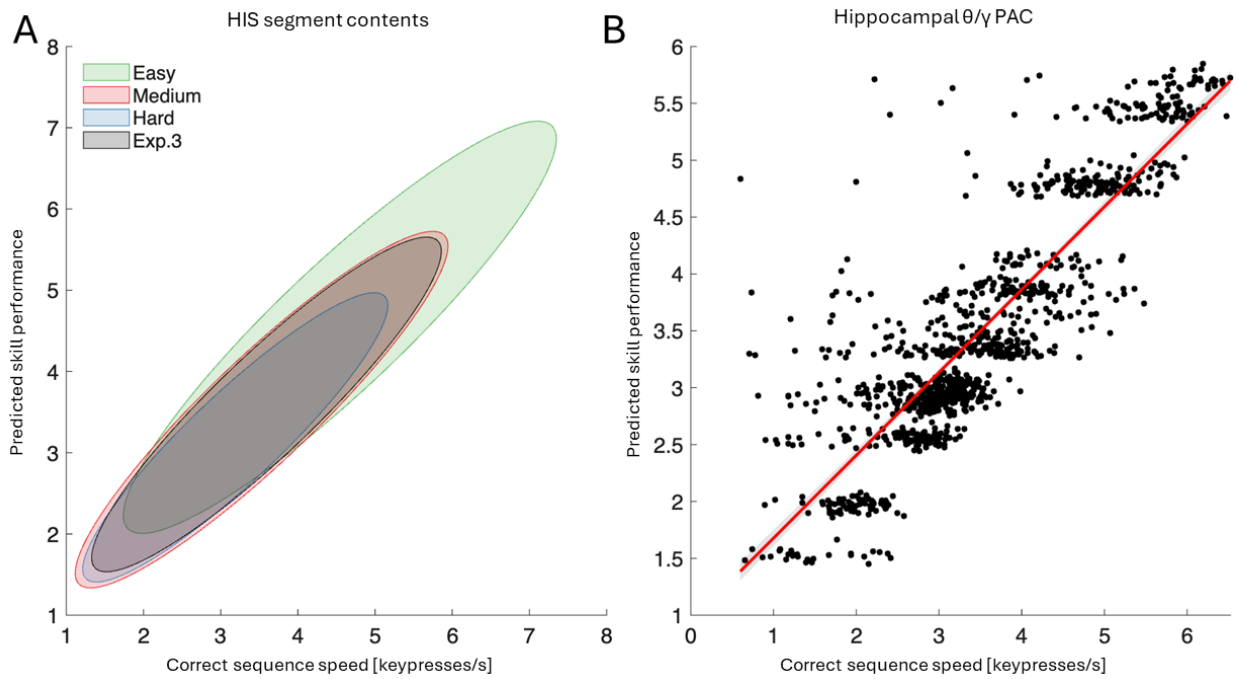

Figure S15: (A) HIS segment content (number of keypresses/HIS segment, fours skill groups, Experiments 2 and 3) were used to model skill performance (speed) using linear-mixed effects models. Note that the actual mean skill speed of practice trials (x-axis) matched closely the speed modeled by HIS segment content (y axis) across the four skill groups tested (Slow: $F_{1,2308}$=37.6, t_{2308}=6.14, p=9.97×10^{-10}, Medium: $F_{1,2456}$=241.2, t_{2456}=15.5, p=5.98×10^{-52}, Fast: $F_{1,3228}$=269.4, t_{3228}=16.4, p=3.34×10^{-58}, and Exp.3: $F_{1,990}$=55.3, t_{990}=7.44, p=2.24×10^{-13}). Thus, during trials with measurable HIS segments, HIS segment content predicted skill levels. **(B)** Hippocampal θ/γ PAC during the initial 4 seconds that encompass HIS segments (Experiment 3) were used to model skill performance (speed) using linear-mixed effects models. Note that the actual mean skill speed of practice trials (x-axis) matched closely the speed modeled by hippocampal θ/γ PAC (y axis, trial 1-36, F_{1061}=6.21, t_{1061}=2.49, p=0.013). Thus, hippocampal θ/γ PAC predicted skill levels across practice trials.

Supplementary Tables

Table S1: Our analysis identified four clustered brain regions contributing to θ/γ PAC difference during HIS segments relative to its time-shifted surrogates (n=200). Tables below document the subregions defined in HCP-MMP atlas contained within each cluster.

(A) Contralateral hippocampal cortex

Hemisphere ("L" or "R")	Area Name	Area Description	t_{31} value	*p* value
R	H	Hippocampus	2.76	3.76×10^{-3}
R	PHA1	ParaHippocampal area 1	3.58	5.77×10^{-4}
R	PHA2	ParaHippocampal area 2	3.98	1.91×10^{-4}
R	PHA3	ParaHippocampal area 3	4.07	1.52×10^{-4}

(B) Contralateral insula and orbitofrontal cortex

Hemisphere ("L" or "R")	Area Name	Area Description	t_{31} value	*p* value
R	13l	Area 13l	3.27	1.30×10^{-3}
R	OFC	Orbitofrontal cortex	3.92	2.29×10^{-4}
R	Pir	Piriform cortex	2.79	4.46×10^{-3}
R	AVI	Anterior Ventral Insular Area	2.87	3.71×10^{-3}
R	AAIC	Anterior Agranular Insula Complex	3.39	9.56×10^{-4}
R	TGd	Area TG dorsal	3.39	9.58×10^{-4}

(C) Bilateral vmPFC

Hemisphere ("L" or "R")	Area Name	Area Description	t_{31} value	*p* value
L	p32	Area p32 prime	2.88	3.58×10^{-3}
L	10r	Area 10r	3.17	1.69×10^{-3}
R	10r	Area 10r	3.30	1.22×10^{-3}

(D) Ipsilateral parieto-occipital regions

Hemisphere	Area Name	Area Description	t_{31} value	*p* value

(“L” or “R”)				
L	V3A	Area V3A	3.49	7.30×10^{-4}
L	POS2	Parieto-Occipital Sulcus Area 2	2.88	3.53×10^{-3}
L	IPS1	IntraParietal Sulcus Area 1	3.03	2.45×10^{-3}
L	DVT	Dorsal Transitional Visual Area	2.93	3.12×10^{-3}
L	V6A	Area V6A	2.91	3.31×10^{-3}

Table S2: Our analysis identified three clustered brain regions contributing to β burst rate difference between HIS and post-HIS segments. Tables below document the subregions defined in HCP-MMP atlas contained within each cluster.

(A) Contralateral insula, frontal and temporal cortex

Hemisphere ("L" or "R")	Area Name	Area Description	t_{31} value	*p* value
R	PEF	Premotor Eye Fields	3.25	1.39×10^{-3}
R	6v	Ventral Area 6	3.64	4.93×10^{-4}
R	8C	Area 8C	2.77	4.73×10^{-3}
R	44	Area 44	2.72	5.24×10^{-3}
R	45	Area 45	3.50	5.25×10^{-4}
R	47l	Area 47l	2.57	7.58×10^{-3}
R	6r	Rostral Area 6	2.94	3.04×10^{-3}
R	IFJa	Area IFJa	2.89	3.48×10^{-3}
R	IFJp	Area IFJp	2.94	3.11×10^{-3}
R	IFSp	Area IFSp	4.21	1.02×10^{-4}
R	IFSa	Area IFSa	3.59	5.63×10^{-4}
R	p9-46v	Area posterior 9-46v	2.85	3.86×10^{-3}
R	47s	Area 47s	2.55	7.98×10^{-3}
R	PoI2	Posterior Insula area 2	3.04	2.42×10^{-3}
R	TA2	Area TA2	3.52	6.78×10^{-4}
R	FOP4	Frontal Opercular Area 4	3.76	3.53×10^{-4}
R	MI	Middle Insular Area	3.04	2.36×10^{-3}
R	Pir	Piriform cortex	3.07	2.21×10^{-3}
R	AVI	Anterior Ventral Insular Area	2.58	7.51×10^{-3}
R	AAIC	Anterior Agranular Insula Complex	4.42	5.57×10^{-5}
R	FOP1	Frontal Opercular Area 1	3.53	6.65×10^{-4}
R	FOP3	Frontal Opercular Area 3	3.53	6.63×10^{-4}
R	STGa	Area STGa	5.81	1.07×10^{-6}
R	A5	Auditory 5 Complex	3.25	1.38×10^{-3}

R	STSda	Area STSd anterior	4.25	9.06×10^{-5}
R	TGd	Area TG dorsal	3.33	1.13×10^{-3}
R	TE2a	Area TE2 anterior	3,86	2.68×10^{-4}
R	PoI1	Area Posterior Insular 1	3.11	1.99×10^{-3}
R	FOP5	Frontal Opercular Area 5	3.51	7.00×10^{-4}
R	p47r	Area posterior 47r	3.76	3.55×10^{-4}
R	STSva	Area STSv anterior	2.92	3.18×10^{-3}
R	TE1m	Area TE1 Middle	2.54	8.13×10^{-3}
R	PI	Para-Insular Area	3.70	4.23×10^{-4}

(B) Bilateral anterior cingulate cortex

Hemisphere ("L" or "R")	Area Name	Area Description	t_{31} value	*p* value
L	d32	Area dorsal 32	3.10	2.07×10^{-3}
L	8BM	Area 8BM	3.69	4.26×10^{-4}
R	a24pr	Anterior 24 prime	3.70	4.09×10^{-4}
R	p32pr	Area p32 prime	2.47	9.51×10^{-3}
R	d32	Area dorsal 32	3.59	5.60×10^{-4}
R	8BM	Area 8BM	2.80	4.41×10^{-3}
R	a32pr	Area anterior 32 prime	3.27	1.33×10^{-3}
R	p24	Area posterior 24	3.04	2.41×10^{-3}

(C) Ipsilateral insula, frontal and temporal cortex

Hemisphere ("L" or "R")	Area Name	Area Description	t_{31} value	*p* value
L	A1	Primary Auditory Cortex	4.37	6.47×10^{-5}
L	44	Area 44	2.59	7.17×10^{-3}
L	43	Area 43	2.71	5.41×10^{-3}
L	OP4	Area OP4/PV	3.44	8.41×10^{-4}
L	OP1	Area OP1/SII	2.95	3.01×10^{-3}

L	OP2-3	Area OP2-3/VS	3.90	2.41×10^{-4}
L	52	Area 52	4.41	5.72×10^{-5}
L	PoI2	Posterior Insular Area 2	4.04	1.66×10^{-4}
L	TA2	Area TA2	3.54	6.44×10^{-4}
L	FOP1	Frontal Opercular Area 1	3.43	8.50×10^{-4}
L	FOP2	Frontal Opercular Area 2	3.14	1.86×10^{-3}
L	STGa	Area STGa	4.42	5.57×10^{-5}
L	PBelt	ParaBelt Complex	2.51	8.65×10^{-3}
L	A5	Auditory 5 Complex	3.40	9.36×10^{-4}
L	STSda	Area STSd anterior	4.83	1.73×10^{-5}
L	TE1a	Area TE1 anterior	2.57	7.62×10^{-3}
L	PFop	Area PF opercular	4.29	8.06×10^{-5}
L	PoI1	Area Posterior Insular 1	3.12	1.96×10^{-3}
L	Ig	Insular Granular Complex	3.24	1.41×10^{-3}
L	MBelt	Medial Belt Complex	4.04	1.64×10^{-4}
L	A4	Auditory 4 Complex	3.00	2.65×10^{-3}
L	STSva	Area STSv anterior	4.15	1.19×10^{-4}
L	TE1m	Area TE1 Middle	2.51	8.66×10^{-3}
L	PI	Para-Insular Area	2.46	9.75×10^{-3}

References

1. Constantinidis, C., and Klingberg, T. (2016). The neuroscience of working memory capacity and training. Nat Rev Neurosci *17*, 438-449. 10.1038/nrn.2016.43.
2. Baddeley, A. (2003). Working memory: looking back and looking forward. Nat Rev Neurosci *4*, 829-839. 10.1038/nrn1201.
3. Borders, A.A., Ranganath, C., and Yonelinas, A.P. (2022). The hippocampus supports high-precision binding in visual working memory. Hippocampus *32*, 217-230. 10.1002/hipo.23401.
4. Sami, S., Robertson, E.M., and Miall, R.C. (2014). The time course of task-specific memory consolidation effects in resting state networks. J Neurosci *34*, 3982-3992. 10.1523/JNEUROSCI.4341-13.2014.
5. Quentin, R., King, J.R., Sallard, E., Fishman, N., Thompson, R., Buch, E.R., and Cohen, L.G. (2019). Differential Brain Mechanisms of Selection and Maintenance of Information during Working Memory. J Neurosci *39*, 3728-3740. 10.1523/JNEUROSCI.2764-18.2019.
6. Szucs-Bencze, L., Vekony, T., Pesthy, O., Szabo, N., Kincses, T.Z., Turi, Z., and Nemeth, D. (2023). Modulating Visuomotor Sequence Learning by Repetitive Transcranial Magnetic Stimulation: What Do We Know So Far? J Intell *11*. 10.3390/jintelligence11100201.
7. Bo, J., and Seidler, R.D. (2009). Visuospatial working memory capacity predicts the organization of acquired explicit motor sequences. J Neurophysiol *101*, 3116-3125. 00006.2009 [pii]

10.1152/jn.00006.2009.
8. Nassar, M.R., Helmers, J.C., and Frank, M.J. (2018). Chunking as a rational strategy for lossy data compression in visual working memory. Psychol Rev *125*, 486-511. 10.1037/rev0000101.
9. Collins, A.G.E., and Frank, M.J. (2018). Within- and across-trial dynamics of human EEG reveal cooperative interplay between reinforcement learning and working memory. Proc Natl Acad Sci U S A *115*, 2502-2507. 10.1073/pnas.1720963115.
10. Collins, A.G., and Frank, M.J. (2012). How much of reinforcement learning is working memory, not reinforcement learning? A behavioral, computational, and neurogenetic analysis. Eur J Neurosci *35*, 1024-1035. 10.1111/j.1460-9568.2011.07980.x.
11. Anguera, J.A., Reuter-Lorenz, P.A., Willingham, D.T., and Seidler, R.D. Contributions of spatial working memory to visuomotor learning. J Cogn Neurosci *22*, 1917-1930. 10.1162/jocn.2009.21351.
12. Cowan, N. (2008). What are the differences between long-term, short-term, and working memory? Prog Brain Res *169*, 323-338. 10.1016/S0079-6123(07)00020-9.
13. Lashley, K.S. (1951). The problem of serial order in behavior. In Cerebral mechanisms in behavior: The Hixon Symposium, L.A. Jeffress, ed. (Wiley), pp. 112-146.
14. Miller, G.A. (1956). The magical number seven plus or minus two: some limits on our capacity for processing information. Psychol Rev *63*, 81-97.
15. Verwey, W.B., and Eikelboom, T. (2003). Evidence for lasting sequence segmentation in the discrete sequence-production task. J Mot Behav *35*, 171-181. 10.1080/00222890309602131.
16. Kennerley, S.W., Sakai, K., and Rushworth, M.F. (2004). Organization of action sequences and the role of the pre-SMA. J Neurophysiol *91*, 978-993. 10.1152/jn.00651.2003

00651.2003 [pii].
17. Allen, J.G., Scovern, A.W., Logue, A.M., and Coyne, L. (1988). Indications for extended psychiatric hospitalization: a study of clinical opinion. Compr Psychiatry *29*, 604-612. 10.1016/0010-440x(88)90081-8.
18. Gobet, F., and Clarkson, G. (2004). Chunks in expert memory: evidence for the magical number four ... or is it two? Memory *12*, 732-747. 10.1080/09658210344000530.
19. Bönstrup, M., Iturrate, I., Thompson, R., Cruciani, G., Censor, N., and Cohen, L.G. (2019). A Rapid Form of Offline Consolidation in Skill Learning. Curr Biol *29*, 1346-1351 e1344. 10.1016/j.cub.2019.02.049.
20. Baddeley, A. (1992). Working memory. Science *255*, 556-559.
21. Bo, J., Jennett, S., and Seidler, R.D. (2011). Working memory capacity correlates with implicit serial reaction time task performance. Exp Brain Res *214*, 73-81. 10.1007/s00221-011-2807-8.
22. Unsworth, N., and Engle, R.W. (2007). The nature of individual differences in working memory capacity: active maintenance in primary memory and controlled search from secondary memory. Psychol Rev *114*, 104-132. 10.1037/0033-295X.114.1.104.
23. Sakai, K., Kitaguchi, K., and Hikosaka, O. (2003). Chunking during human visuomotor sequence learning. Exp Brain Res *152*, 229-242. 10.1007/s00221-003-1548-8.
24. Branscheidt, M., Kassavetis, P., Anaya, M., Rogers, D., Huang, H.D., Lindquist, M.A., and Celnik, P. (2019). Fatigue induces long-lasting detrimental changes in motor-skill learning. Elife *8*. 10.7554/eLife.40578.
25. Bachinger, M., Lehner, R., Thomas, F., Hanimann, S., Balsters, J., and Wenderoth, N. (2019). Human motor fatigability as evoked by repetitive movements results from a gradual breakdown of surround inhibition. Elife *8*. 10.7554/eLife.46750.
26. Sharples, S.A., Gould, J.A., Vandenberk, M.S., and Kalmar, J.M. (2016). Cortical Mechanisms of Central Fatigue and Sense of Effort. PLoS One *11*, e0149026. 10.1371/journal.pone.0149026.
27. Hull, C.L. (1943). Principles of behavior (Appleton-Century- Crofts).
28. Kay, H. (1956). What do we learn? Proc R Soc Med *49*, 1021-1023. 10.1177/003591575604901212.
29. Daume, J., Kaminski, J., Schjetnan, A.G.P., Salimpour, Y., Khan, U., Kyzar, M., Reed, C.M., Anderson, W.S., Valiante, T.A., Mamelak, A.N., and Rutishauser, U. (2024). Control of working memory by phase-amplitude coupling of human hippocampal neurons. Nature *629*, 393-401. 10.1038/s41586-024-07309-z.
30. Foster, D.J., and Wilson, M.A. (2007). Hippocampal theta sequences. Hippocampus *17*, 1093-1099. 10.1002/hipo.20345.
31. Skaggs, W.E., McNaughton, B.L., Wilson, M.A., and Barnes, C.A. (1996). Theta phase precession in hippocampal neuronal populations and the compression of temporal sequences. Hippocampus *6*, 149-172. 10.1002/(SICI)1098-1063(1996)6:2<149::AID-HIPO6>3.0.CO;2-K.
32. Zheng, J., Yebra, M., Schjetnan, A.G.P., Patel, K., Katz, C.N., Kyzar, M., Mosher, C.P., Kalia, S.K., Chung, J.M., Reed, C.M., et al. (2024). Theta phase precession supports memory formation and retrieval of naturalistic experience in humans. Nat Hum Behav *8*, 2423-2436. 10.1038/s41562-024-01983-9.
33. Kaminski, J., Brzezicka, A., and Wrobel, A. (2011). Short-term memory capacity (7 +/- 2) predicted by theta to gamma cycle length ratio. Neurobiol Learn Mem *95*, 19-23. 10.1016/j.nlm.2010.10.001.

34. Lisman, J.E., and Jensen, O. (2013). The theta-gamma neural code. Neuron *77*, 1002-1016. 10.1016/j.neuron.2013.03.007.
35. Griffiths, B.J., Mayhew, S.D., Mullinger, K.J., Jorge, J., Charest, I., Wimber, M., and Hanslmayr, S. (2019). Alpha/beta power decreases track the fidelity of stimulus-specific information. Elife *8*. 10.7554/eLife.49562.
36. Hanslmayr, S., Staudigl, T., and Fellner, M.C. (2012). Oscillatory power decreases and long-term memory: the information via desynchronization hypothesis. Front Hum Neurosci *6*, 74. 10.3389/fnhum.2012.00074.
37. Griffiths, B.J., Martin-Buro, M.C., Staresina, B.P., and Hanslmayr, S. (2021). Disentangling neocortical alpha/beta and hippocampal theta/gamma oscillations in human episodic memory formation. Neuroimage *242*, 118454. 10.1016/j.neuroimage.2021.118454.
38. Kavanaugh, B.C., Vigne, M.M., Thorpe, R., Legere, C., Acuff, W.L., Vaughan, N., Tirrell, E., Haegens, S., Carpenter, L.L., and Jones, S.R. (2025). The Association between Oscillatory Burst Features and Human Working Memory Accuracy. J Cogn Neurosci, 1-18. 10.1162/jocn.a.87.
39. Lundqvist, M., Rose, J., Herman, P., Brincat, S.L., Buschman, T.J., and Miller, E.K. (2016). Gamma and Beta Bursts Underlie Working Memory. Neuron *90*, 152-164. 10.1016/j.neuron.2016.02.028.
40. Liljefors, J., Almeida, R., Rane, G., Lundstrom, J.N., Herman, P., and Lundqvist, M. (2024). Distinct functions for beta and alpha bursts in gating of human working memory. Nat Commun *15*, 8950. 10.1038/s41467-024-53257-7.
41. Enoka, R.M., and Duchateau, J. (2016). Translating Fatigue to Human Performance. Med Sci Sports Exerc *48*, 2228-2238. 10.1249/MSS.0000000000000929.
42. Seidler, R.D., Bernard, J.A., Burutolu, T.B., Fling, B.W., Gordon, M.T., Gwin, J.T., Kwak, Y., and Lipps, D.B. Motor control and aging: links to age-related brain structural, functional, and biochemical effects. Neurosci Biobehav Rev *34*, 721-733. S0149-7634(09)00159-6 [pii]

10.1016/j.neubiorev.2009.10.005.
43. Ariani, G., and Diedrichsen, J. (2019). Sequence learning is driven by improvements in motor planning. J Neurophysiol *121*, 2088-2100. 10.1152/jn.00041.2019.
44. Heusser, A.C., Poeppel, D., Ezzyat, Y., and Davachi, L. (2016). Episodic sequence memory is supported by a theta-gamma phase code. Nat Neurosci *19*, 1374-1380. 10.1038/nn.4374.
45. Abubaker, M., Al Qasem, W., Pilatova, K., Jezdik, P., and Kvasnak, E. (2024). Theta-gamma-coupling as predictor of working memory performance in young and elderly healthy people. Mol Brain *17*, 74. 10.1186/s13041-024-01149-8.
46. Acuna, D.E., Wymbs, N.F., Reynolds, C.A., Picard, N., Turner, R.S., Strick, P.L., Grafton, S.T., and Kording, K.P. (2014). Multifaceted aspects of chunking enable robust algorithms. J Neurophysiol *112*, 1849-1856. 10.1152/jn.00028.2014.
47. Ramkumar, P., Acuna, D.E., Berniker, M., Grafton, S.T., Turner, R.S., and Kording, K.P. (2016). Chunking as the result of an efficiency computation trade-off. Nat Commun *7*, 12176. 10.1038/ncomms12176.
48. Wright, D.L., Rhee, J.H., and Vaculin, A. (2010). Offline improvement during motor sequence learning is not restricted to developing motor chunks. J Mot Behav *42*, 317-324. 10.1080/00222895.2010.510543.
49. Terrace, H.S., Son, L.K., and Brannon, E.M. (2003). Serial expertise of rhesus macaques. Psychol Sci *14*, 66-73. 10.1111/1467-9280.01420.

50. Feldmann-Wustefeld, T., and Vogel, E.K. (2019). Neural Evidence for the Contribution of Active Suppression During Working Memory Filtering. Cereb Cortex *29*, 529-543. 10.1093/cercor/bhx336.
51. Jiang, D., and Kalyuga, S. (2022). Learning English as a Foreign Language Writing Skills in Collaborative Settings: A Cognitive Load Perspective. Front Psychol *13*, 932291. 10.3389/fpsyg.2022.932291.
52. Bo, J., Borza, V., and Seidler, R.D. (2009). Age-related declines in visuospatial working memory correlate with deficits in explicit motor sequence learning. J Neurophysiol *102*, 2744-2754. 00393.2009 [pii]

10.1152/jn.00393.2009.
53. Xu, J., Mawase, F., and Schieber, M.H. (2024). Evolution, biomechanics, and neurobiology converge to explain selective finger motor control. Physiol Rev *104*, 983-1020. 10.1152/physrev.00030.2023.
54. Beck, S., and Hallett, M. (2010). Surround inhibition is modulated by task difficulty. Clin Neurophysiol *121*, 98-103. S1388-2457(09)00539-2 [pii]

10.1016/j.clinph.2009.09.010.
55. Dash, D., Iwane, F., Hayward, W., Salamanca-Giron, R., Bönstrup, M., Buch, E., and Cohen, L.G. (2025). Sequence action representations contextualize during rapid skill learning. bioRxiv, 2024.2008.2015.608189. 10.1101/2024.08.15.608189.
56. Pan, S.C., and Rickard, T.C. (2015). Sleep and motor learning: Is there room for consolidation? Psychol Bull *141*, 812-834. 10.1037/bul0000009.
57. Nieuwenhuis, S., Ridderinkhof, K.R., de Jong, R., Kok, A., and van der Molen, M.W. (2000). Inhibitory inefficiency and failures of intention activation: age-related decline in the control of saccadic eye movements. Psychol Aging *15*, 635-647.
58. Rozand, V., Pageaux, B., Marcora, S.M., Papaxanthis, C., and Lepers, R. (2014). Does mental exertion alter maximal muscle activation? Front Hum Neurosci *8*, 755. 10.3389/fnhum.2014.00755.
59. Enoka, R.M., and Duchateau, J. (2008). Muscle fatigue: what, why and how it influences muscle function. J Physiol *586*, 11-23. 10.1113/jphysiol.2007.139477.
60. Gandevia, S.C. (2001). Spinal and supraspinal factors in human muscle fatigue. Physiol Rev *81*, 1725-1789. 10.1152/physrev.2001.81.4.1725.
61. Verwey, W.B., and Dronkert, Y. (1996). Practicing a Structured Continuous Key-Pressing Task: Motor Chunking or Rhythm Consolidation? J Mot Behav *28*, 71-79. 10.1080/00222895.1996.9941735.
62. Hikosaka, O., Nakahara, H., Rand, M.K., Sakai, K., Lu, X., Nakamura, K., Miyachi, S., and Doya, K. (1999). Parallel neural networks for learning sequential procedures. Trends Neurosci *22*, 464-471.
63. Shea, C.H., Park, J.H., and Braden, H.W. (2006). Age-related effects in sequential motor learning. Phys Ther *86*, 478-488.
64. Abrahamse, E.L., Jimenez, L., Verwey, W.B., and Clegg, B.A. (2010). Representing serial action and perception. Psychon Bull Rev *17*, 603-623. 10.3758/PBR.17.5.603.
65. Seidler, R.D., Bo, J., and Anguera, J.A. (2012). Neurocognitive contributions to motor skill learning: the role of working memory. J Mot Behav *44*, 445-453. 10.1080/00222895.2012.672348.
66. McDougle, S.D., and Hillman, H. (2025). Motor working memory. Trends Cogn Sci. 10.1016/j.tics.2025.08.011.

67. Griffiths, B.J., Parish, G., Roux, F., Michelmann, S., van der Plas, M., Kolibius, L.D., Chelvarajah, R., Rollings, D.T., Sawlani, V., Hamer, H., et al. (2019). Directional coupling of slow and fast hippocampal gamma with neocortical alpha/beta oscillations in human episodic memory. Proc Natl Acad Sci U S A *116*, 21834-21842. 10.1073/pnas.1914180116.
68. Parish, G., Hanslmayr, S., and Bowman, H. (2018). The Sync/deSync Model: How a Synchronized Hippocampus and a Desynchronized Neocortex Code Memories. J Neurosci *38*, 3428-3440. 10.1523/JNEUROSCI.2561-17.2018.
69. Hanslmayr, S., Staresina, B.P., and Bowman, H. (2016). Oscillations and Episodic Memory: Addressing the Synchronization/Desynchronization Conundrum. Trends Neurosci *39*, 16-25. 10.1016/j.tins.2015.11.004.
70. Griffiths, B.J., and Fuentemilla, L. (2020). Event conjunction: How the hippocampus integrates episodic memories across event boundaries. Hippocampus *30*, 162-171. 10.1002/hipo.23161.
71. Herman, P.A., Lundqvist, M., and Lansner, A. (2013). Nested theta to gamma oscillations and precise spatiotemporal firing during memory retrieval in a simulated attractor network. Brain Res *1536*, 68-87. 10.1016/j.brainres.2013.08.002.
72. Lundqvist, M., Herman, P., and Lansner, A. (2011). Theta and gamma power increases and alpha/beta power decreases with memory load in an attractor network model. J Cogn Neurosci *23*, 3008-3020. 10.1162/jocn_a_00029.
73. Mi, Y., Katkov, M., and Tsodyks, M. (2017). Synaptic Correlates of Working Memory Capacity. Neuron *93*, 323-330. 10.1016/j.neuron.2016.12.004.
74. Lisman, J.E., and Idiart, M.A. (1995). Storage of 7 +/- 2 short-term memories in oscillatory subcycles. Science *267*, 1512-1515. 10.1126/science.7878473.
75. Jensen, O., and Lisman, J.E. (2005). Hippocampal sequence-encoding driven by a cortical multi-item working memory buffer. Trends Neurosci *28*, 67-72. 10.1016/j.tins.2004.12.001.
76. Colgin, L.L. (2015). Theta-gamma coupling in the entorhinal-hippocampal system. Curr Opin Neurobiol *31*, 45-50. 10.1016/j.conb.2014.08.001.
77. Buch, E.R., Claudino, L., Quentin, R., Bönstrup, M., and Cohen, L.G. (2021). Consolidation of human skill linked to waking hippocampo-neocortical replay. Cell Rep *35*, 109193. 10.1016/j.celrep.2021.109193.
78. Griffin, S., Khanna, P., Choi, H., Thiesen, K., Novik, L., Morecraft, R.J., and Ganguly, K. (2025). Ensemble reactivations during brief rest drive fast learning of sequences. Nature. 10.1038/s41586-024-08414-9.
79. Jacobacci, F., Armony, J.L., Yeffal, A., Lerner, G., Amaro, E., Jr., Jovicich, J., Doyon, J., and Della-Maggiore, V. (2020). Rapid hippocampal plasticity supports motor sequence learning. Proc Natl Acad Sci U S A *117*, 23898-23903. 10.1073/pnas.2009576117.
80. Mylonas, D., Schapiro, A.C., Verfaellie, M., Baxter, B., Vangel, M., Stickgold, R., and Manoach, D.S. (2024). Maintenance of Procedural Motor Memory across Brief Rest Periods Requires the Hippocampus. J Neurosci *44*. 10.1523/JNEUROSCI.1839-23.2024.
81. Hayward, W., Buch, E.R., Norato, G., Iwane, F., Dash, D., Salamanca-Giron, R.F., Bartrum, E., Walitt, B., Nath, A., and Cohen, L.G. (2024). Procedural Motor Memory Deficits in Patients With Long-COVID. Neurology *102*, e208073. 10.1212/WNL.0000000000208073.
82. Brooks, E., Wallis, S., Hendrikse, J., and Coxon, J. (2024). Micro-consolidation occurs when learning an implicit motor sequence, but is not influenced by HIIT exercise. NPJ Sci Learn *9*, 23. 10.1038/s41539-024-00238-6.
83. Gillespie, A.K., Astudillo Maya, D.A., Denovellis, E.L., Liu, D.F., Kastner, D.B., Coulter, M.E., Roumis, D.K., Eden, U.T., and Frank, L.M. (2021). Hippocampal replay reflects specific past

experiences rather than a plan for subsequent choice. Neuron. 10.1016/j.neuron.2021.07.029.
84. Chen, P.C., Stritzelberger, J., Walther, K., Hamer, H., and Staresina, B.P. (2025). Hippocampal ripples during offline periods predict human motor sequence learning. J Neurosci. 10.1523/JNEUROSCI.1502-25.2025.
85. Sjogard, M., Baxter, B., Mylonas, D., Thompson, M., Kwok, K., Driscoll, B., Tolosa, A., Shi, W., Stickgold, R., Vangel, M., et al. (2025). Hippocampal ripples predict motor learning during brief rest breaks in humans. Nat Commun *16*, 6089. 10.1038/s41467-025-61136-y.
86. Albouy, G., King, B.R., Maquet, P., and Doyon, J. (2013). Hippocampus and striatum: dynamics and interaction during acquisition and sleep-related motor sequence memory consolidation. Hippocampus *23*, 985-1004. 10.1002/hipo.22183.
87. Lundqvist, M., Herman, P., Warden, M.R., Brincat, S.L., and Miller, E.K. (2018). Gamma and beta bursts during working memory readout suggest roles in its volitional control. Nat Commun *9*, 394. 10.1038/s41467-017-02791-8.
88. Eysenck, H.J. (1965). A Three-Factor Theory of Reminiscence. Br J Psychol *56*, 163-182. 10.1111/j.2044-8295.1965.tb00956.x.
89. Torok, B., Janacsek, K., Nagy, D.G., Orban, G., and Nemeth, D. (2017). Measuring and filtering reactive inhibition is essential for assessing serial decision making and learning. J Exp Psychol Gen *146*, 529-542. 10.1037/xge0000288.
90. Karni, A., Meyer, G., Jezzard, P., Adams, M.M., Turner, R., and Ungerleider, L.G. (1995). Functional MRI evidence for adult motor cortex plasticity during motor skill learning. Nature *377*, 155-158. 10.1038/377155a0.
91. Walker, M.P., and Stickgold, R. (2004). Sleep-dependent learning and memory consolidation. Neuron *44*, 121-133.
92. Iwane, F., Dash, D., Salamanca-Giron, R.F., Hayward, W., Bönstrup, M., Buch, E.R., and Cohen, L.G. (2023). Combined low-frequency brain oscillatory activity and behavior predict future errors in human motor skill. Curr Biol *33*, 3145-3154 e3145. 10.1016/j.cub.2023.06.040.
93. Blischke, K., and Malangre, A. (2016). Chunk concatenation evolves with practice and sleep-related enhancement consolidation in a complex arm movement sequence. J Hum Kinet *51*, 5-17. 10.1515/hukin-2015-0163.
94. Song, S., and Cohen, L. (2014). Impact of conscious intent on chunking during motor learning. Learn Mem *21*, 449-451. 10.1101/lm.035824.114.
95. Tosatto, L., Fagot, J., Nemeth, D., and Rey, A. (2022). The Evolution of Chunks in Sequence Learning. Cogn Sci *46*, e13124. 10.1111/cogs.13124.
96. Oostenveld, R., Fries, P., Maris, E., and Schoffelen, J.-M. (2011). FieldTrip: open source software for advanced analysis of MEG, EEG, and invasive electrophysiological data. Computational intelligence and neuroscience *2011*, 1-9.
97. Fischl, B. (2012). FreeSurfer. Neuroimage *62*, 774-781. 10.1016/j.neuroimage.2012.01.021.
98. Marcus, D.S., Harwell, J., Olsen, T., Hodge, M., Glasser, M.F., Prior, F., Jenkinson, M., Laumann, T., Curtiss, S.W., and Van Essen, D.C. (2011). Informatics and data mining tools and strategies for the human connectome project. Front Neuroinform *5*, 4. 10.3389/fninf.2011.00004.
99. Delorme, A., and Makeig, S. (2004). EEGLAB: an open source toolbox for analysis of single-trial EEG dynamics including independent component analysis. Journal of neuroscience methods *134*, 9-21.

100. Tort, A.B., Komorowski, R., Eichenbaum, H., and Kopell, N. (2010). Measuring phase-amplitude coupling between neuronal oscillations of different frequencies. J Neurophysiol *104*, 1195-1210. 10.1152/jn.00106.2010.
101. Vaz, A.P., Yaffe, R.B., Wittig, J.H., Jr., Inati, S.K., and Zaghloul, K.A. (2017). Dual origins of measured phase-amplitude coupling reveal distinct neural mechanisms underlying episodic memory in the human cortex. Neuroimage *148*, 148-159. 10.1016/j.neuroimage.2017.01.001.
102. Norman, Y., Yeagle, E.M., Khuvis, S., Harel, M., Mehta, A.D., and Malach, R. (2019). Hippocampal sharp-wave ripples linked to visual episodic recollection in humans. Science *365*. 10.1126/science.aax1030.
103. Aru, J., Aru, J., Priesemann, V., Wibral, M., Lana, L., Pipa, G., Singer, W., and Vicente, R. (2015). Untangling cross-frequency coupling in neuroscience. Curr Opin Neurobiol *31*, 51-61. 10.1016/j.conb.2014.08.002.
104. Shin, H., Law, R., Tsutsui, S., Moore, C.I., and Jones, S.R. (2017). The rate of transient beta frequency events predicts behavior across tasks and species. Elife *6*. 10.7554/eLife.29086.
105. Maris, E., and Oostenveld, R. (2007). Nonparametric statistical testing of EEG- and MEG-data. J Neurosci Methods *164*, 177-190. 10.1016/j.jneumeth.2007.03.024.
106. Wymbs, N.F., Bassett, D.S., Mucha, P.J., Porter, M.A., and Grafton, S.T. (2012). Differential recruitment of the sensorimotor putamen and frontoparietal cortex during motor chunking in humans. Neuron *74*, 936-946. 10.1016/j.neuron.2012.03.038.